UNIVERSIDADE D
COIMBRA

Gabriela Meurer Lemes

Thermal Performance Evaluation of Lightweight Steel Frame Walls

Dissertação de Mestrado em Eficiência Acústica e Energética para uma Construção Sustentável, orientada pelo Professor Doutor Paulo Fernando Antunes dos Santos e Professor Doutor Diogo Manuel Rosa Mateus e apresentada ao Departamento de Engenharia Civil da Faculdade de Ciências e Tecnologia da Universidade de Coimbra

Março de 2020

Faculdade de Ciências e Tecnologia da Universidade de Coimbra
Departamento de Engenharia Civil

Gabriela Meurer Lemes

THERMAL PERFORMANCE EVALUATION OF LIGHTWEIGHT STEEL FRAME WALLS

AVALIAÇÃO DO DESEMPENHO TÉRMICO DE PAREDES EM LIGHTWEIGHT STEEL FRAME

Dissertação de Mestrado em Eficiência Acústica e Energética para uma Construção Sustentável,
orientada pelo Professor Doutor Paulo Fernando Antunes dos Santos e pelo Professor Doutor Diogo Manuel Rosa Mateus.

Março de 2020

UNIVERSIDADE D
COIMBRA

ACKNOWLEDGEMENTS

I am grateful to my family and friends for the emotional support and for believing in my potentials to achieve this goal.

I would also like to thank my advisors, Professor Paulo Santos and Professor Diogo Mateus, for their valuable technical support, critical analysis and for their confidence in my work as a member of the Tyre4BuildIns project during the last year.

This dissertation is part of the research project Tyre4BuildIns – "Recycled tyre rubber resin-bonded for building insulation systems towards energy efficiency" – is supported by FEDER funds through the Competitivity Factors Operational Programme – COMPETE – and by national funds through Foundation for Science and Technology – FCT – within the scope of the project POCI-01-0145-FEDER-032061.

RESUMO

Atualmente, alcançar um alto nível de eficiência energética no o setor de edifícios é imperativo, devendo o consumo de energia na operação ser reduzido para níveis mínimos. Para atingir esse baixo consumo de energia é crucial entender como ocorrem a transferência de calor em todos os tipos de parede, sendo capaz de melhorar o comportamento térmico, reduzindo a perda de calor e diminuindo seu coeficiente de transmissão térmica (valor de U). Para isso, é fundamental uma avaliação precisa e confiável do coeficiente transmissão térmica da envolvente do edifício a fim de se obter uma avaliação consistente do comportamento térmico e, por consequência, da eficiência energética. A construção em Light Steel Frame (LSF) está a ganhar espaço e sendo cada vez mais utilizada devido às suas vantagens conhecidas, tais como ser mais flexível, mais rápida e mais limpa do que o sistema de construção tradicional. No entanto, os elementos construtivos em LSF precisam ser bem projetados e protegidos contra pontes térmicas indesejadas causadas pela alta condutividade térmica do aço. Além disso, avaliar o desempenho térmico das paredes em LSF é uma questão desafiadora, pois sua estrutura interna de aço pode facilmente levar a ocorrência de pontes térmicas que podem induzir a erros de cálculos nos métodos simplificados. Nesta dissertação, simulações numéricas serão realizadas para avaliar diferentes configurações de dois tipos de paredes LSF: uma parede divisória interna e uma parede externa de fachada. Vários parâmetros foram avaliados separadamente para medir sua influência no valor de U da parede, bem como foi também mensurada a eficiência da adição de outros elementos (tiras de corte térmico) com o objetivo de melhorar o desempenho térmico das paredes. Além disso, seis métodos analíticos, disponíveis na literatura, para calcular o valor de U tiveram sua precisão avaliada e comparada. Foram avaliados 80 diferentes modelos de paredes em LSF, utilizando os métodos analíticos, e os valores de U obtidos para cada dos métodos foram comparados com os valores fornecidos pela simulação numérica (THERM), utilizados como valores de referência. A confiabilidade desses modelos numéricos foi assegurada pela comparação com os valores obtidos em uma validação experimental de laboratório.

Palavras-chave: performance térmica; paredes em LSF; divisória interna; parede de fachada; métodos analíticos, valor de U.

ABSTRACT

Nowadays, having a high level of energy efficiency for building sector is mandatory, and the operation energy consumption must be reduced to minimum levels. To achieve this low energy consumption is crucial to understand how heat transfer occurs in every kind of wall, being able to improve the thermal behavior, reducing the heat loss and decreasing its thermal transmittance (U-value). For this, a precise and reliable evaluation of the thermal transmittance of building envelope is fundamental to perform a consistent assessment of thermal behavior and energy efficiency. The light steel frame (LSF) construction is becoming widely used due to its well-known advantages such as being more flexible, faster and cleaner than the traditional construction system. However, these LSF elements need to be well designed and protected against undesired thermal bridges caused by the steel high thermal conductivity. Also, evaluating the thermal performance of LSF walls is a challenging issue as their internal steel structure can easily lead to thermal bridges which may induce calculation mistakes on simplified methods. In this dissertation, numerical simulations are performed to assess different configurations of two kinds of LSF walls: an interior partition wall and an exterior facade wall. Several parameters were evaluated separately to measure their influence on the wall U-value, as well as the addition of other elements (thermal breaks strips) to achieve better thermal performances. Also, six analytical methods, available in literature, to calculate U-value have their accuracy evaluated and compared. 80 different LSF models were evaluated using the analytical methods and the obtained U-values for each one was compared with those provided by numerical simulation (THERM), which were used as the reference value. The reliability of these numerical models was ensuring by comparison with the values given on laboratory experimental validation.

Keywords: thermal performance; LSF walls; interior partition; facade walls; analytical methods; U-value.

TABLE OF CONTENTS

LIST OF FIGURES

LIST OF TABLES

NOMENCLATURE

Symbols

R	thermal resistance [m^2.K/W]
f	fractional area [---]
U	thermal transmittance [W/(m^2.K)]
p	weight factor for the Gorgolewski method [---]
L	flange width [m]
s	stud spacing [m]
sd	stud depth [m]
zf	zone factor [---]
λ	thermal conductivity [W/(m.K)]
r	thermal resistivity [m. K/W]
d	layer sheathing thickness [m]
a	width of section A (thickness of the steel stud web) [m]
b	width of section B (wall insulation cavity) [m]
W	section W [---]
CAV	section CAV [---]
w	width of section W (steel stud influence zone) [m]
cav	width of section CAV (the remaining wall cavity zone) [m]

Subscripts

tot	total
si	internal surface
se	external surface
j	layers, planes (1, 2, 3, …)
n	number of layers or planes
i	sections, paths (A, B, C, …)
q	number of sections or paths
upper	upper limit
lower	lower limit
tot	total value
sheat	sheathing
ins	insulation
thicker	thicker sheathing side (interior or exterior)
met	metal

ABBREVIATIONS

LSF	Lightweight Steel Frame
FEM	Finite Element Method
ISO	International Standards Organization
ASHRAE	American Society of Heating, Refrigerating and Air-conditioning Engineers
OSB	Oriented Strand Board
GPB	Gypsum Plasterboard
EPS	Expanded Polystyrene
ETICS	External Thermal Insulation Composite System
MW	Mineral Wool
HFM	Heat Flow Meter
GHP	Guarded Hot Plate
CHB	Calibrated Hot Box
GHB	Guarded Hot Box
IRT	Infrared Thermography
AIB	Aerogel Insulation Blanket
ICB	Insulation Cork Board
CBW	Cement Wood Board
FCB	Fiber Cement Board
GRB	Glassfiber Reinforced Board
TC	Thermocouples
RMSE	Root Mean Square Error
MaxPE	Maximum Positive Error
MaxNE	Maximum Negative Error
FEM	Finite Element Method

1 INTRODUCTION

1.1 Framework and Motivation

Nowadays, there is a great call to protect the environment and conserve natural resources, as the world is facing a climate change related to global warming. Energy saving has become a new strategic goal in all energy consumer's sectors. In Europe, the building sector account for almost of 40% of the total energy consumption and about 36% of CO_2 emissions (European Union, 2018).

The buildings sector includes energy used in residential, commercial and institutional buildings, and non-specified others. Building energy use includes space heating and cooling, water heating, lighting, appliances and cooking equipment (IEA - International Energy Agency, 2016). In 2016, 39.5% of the energy worldwide was used to heat and cool buildings. In the same year, the amounts of energy used to control the temperature of residential and commercial buildings were 4.93 and 4.42 trillion kWh, respectively (IEA - International Energy Agency, 2018).

The building energy efficiency can be achieved by implementing either active and/or passive energy efficient strategies. Improvements to heating, ventilation and air conditioning (HVAC[1]) systems, lighting, etc., can be considered as active strategies, while improvements on building envelope elements can be considered as passive strategies (Sadineni et al., 2011).

According to Aslani et al. (Aslani et al., 2019), a building envelope is the physical separation between indoor and outdoor environments of a building and are composed by building elements including external walls, floors, ceilings, roof coverings, windows and doors. Besides bounding the conditioned from unconditioned environment, the building envelope protects it from heat, noise, light, wind and water, providing internal thermal and acoustic comfort.

[1] Heating, ventilation and air conditioning.

The acoustic and energy efficiency provided by building envelopes depends on the characteristics and proprieties of every element materials and are important aspects that influencing thermal energy consumed by cooling and heating equipment during the whole year (Abu-Jdayil et al., 2019).

Several factors such as the type of the building, its age, the climate, construction technique, geographical location, electric equipment and residents' behaviour affect the amount of energy demand for a dwelling during its life time (Aslani et al., 2019). Most of this energy, ranging from nearly 50% (Pulselli et al., 2009) up to 60% (Kaynakli, 2012), is used by air-conditioning systems to achieve thermal comfort inside the buildings. In contrast, the efficiency of the building envelope defines how much heat will be gained or lost through it, and this heat transfer rate depends mostly on the thermal transmittance (U-value) of the building element (opaque or translucent) (Soares et al., 2019).

Thermal loses through thermal bridges often lead to building pathologies generated by moisture condensations. So, it is very important to consider the thermal bridges in the building design phase in order to avoid heat losses preventing the pathologies to happen (Tadeu et al., 2011).

Some alternative for the traditional building construction has emerged in recent years and the use of lightweight steel frame (LSF) construction is increasing every year, mostly because its great advantages, such as: cost efficiency, reduced weight, mechanical resistance, fast assemblage, etc. However, the high thermal conductivity of the steel could lead to thermal bridges and a poor thermal performance of the building if it is not properly addressed.

1.2 Objectives

The main objective of this dissertation is to perform a thermal performance evaluation on lightweight steel frame (LSF) walls through different approaches that will be presented in two studies. The first study performs a parametric evaluation using numerical simulations to assess two kinds of LSF walls: an interior partition and an exterior facade. The second study brings a comparison of the accuracy of six analytical methodologies to calculate the thermal transmittance of LSF walls.

Also is part of this dissertation to introduce a state-of-the-art about the theme: lightweight steel framing (LSF) construction and the methods to calculate thermal transmission and thermal performance of LSF construction elements.

To achieve this, the evaluation techniques that will be used are: analytical approach, 2D numerical simulations and laboratorial experimental measurements. The strategy to mitigate thermal bridges evaluated will be the usage of thermal break strips made of different materials available on the market (recycled tyre rubber, cork and aerogel strips)

1.3 Document Organization

This document is organized in five chapters and in this section will be quickly described each one of them.

In the first chapter, the Introduction, are made the initial considerations, motivation and the objectives of the work to be presented. The State-of-the-Art is presented on chapter 2, where the bibliography used to the development of this work is presented and a review of important and relevant works about thermal performance of buildings, thermal transmission evaluation, Lightweight Steel Frame (LSF) construction and analytical calculation methodology.

The following two chapters (3 and 4) provide a description of the practical work performed, where two different approaches regarding the thermal performance of LSF walls are presented, therefore this part is organized into two chapters. In Chapter 3 is reported a study about a comparison between the thermal performance of two types of LSF walls: exterior facade and interior partition. Chapter 4 describes a study case about a comparison between different analytical methods to compute the thermal transmittance value for LSF walls.

And finally, in chapter 5, the Conclusions which summarize the main results of this work are going to be presented.

2 BUILDINGS' EFFICIENCY AND LSF CONSTRUCTION

2.1 Introduction

Due to the current environmental issues there is a global concern to improve the energy efficiency and energy savings on building sector. Buildings energy efficiency can be achieved through optimizing the building shape and form, improving the buildings envelope, using more efficient electric devices, using alternatives energy systems and, by improving the occupant's behaviours (Harvey, 2009).

Building envelope comprise a configuration of building materials, the thermophysical properties of which determine the climatic response of the envelope. According to Rowley (Rowley & Algren, 1937) a building can lose heat by two distinct processes: by conduction through the building envelope and by air infiltrations or leakages. Even though, the building envelope is the principal responsible for the heat losses through the building and its ability to transfer heat is measured and expresses as the thermal transmittance value (U-value).

The U-value of a building envelope is the most important parameter to calculate the thermal transfer of a constructive element allowing to predict the thermal behaviour of the buildings and the energy needs for heating and cooling spaces. To reach energy efficiency it is crucial to characterize the thermal performance of the building envelope at early design stage. Providing a high-performance envelope is one of the most important factors in the design of low-energy buildings, not only because it reduces the energy needs for heating and cooling systems, but also because it permits alternative and more efficient low-energies (downsized) systems to be used (Harvey, 2009).

LSF construction system has emerged as a viable alternative to the traditional construction and its usage are increasing every year, mostly because of its great advantages against the conventional concrete structure and masonry brick system (P. Santos et al., 2020). On this chapter, it will be presented an introduction of the Lightweight Steel Frame (LSF) construction system, its characteristics and its thermal performance analyses and also a quick review about the thermal transmission analytical calculation for construction elements.

2.2 Thermal Behaviour of Buildings

Thermal behaviour of the building quantifies the ability of the building to maintain comfortable inside condition, although outside conditions – temperature, humidity and air velocity – varies from season to season. A building gains heat from solar radiation and loses (or also gain) heat to the environment by convection, depending upon the outside conditions (Vijayalakshmi et al., 2006). The heat transfer between the outer and inner surface of the wall depends on the thermal transmittance of the building envelope. The thermal balance between the inner surface and room inside environment is determined by the thermal radiation and convective heat transfer of the inner surface.

According to Oktay et al., the dynamic thermal characteristics of the building components are influenced by effective parameters, which can be categorized as (*i*) environmental parameters (ambient air temperature, solar heat flux, ventilation, etc.), (*ii*) design parameters (orientation, solar absorptivity, emissivity, etc.) and (*iii*) thermophysical properties for a given building locating in a specific region (Oktay et al., 2017)

Also in a dynamically perspective, two important parameters are used to evaluate the thermal performance of walls: (*i*) the time lag and (*ii*) the decrement factor. They are very important thermal performance characteristics that influence the heat storage capabilities of any materials and can be obtained based on the thermophysical properties of the materials. These are influenced by the external and internal surface temperatures of the wall. In general, higher time lag and lower decrement factor is the preferred thermal performance in tropical regions to minimize energy consumption. Thermal time lag (expressed in hours) is the time delay between the occurrence of maximum temperature at the inside and outside of wall surface during periodic flow of heat. The decrement factor (or attenuation factor) is the ratio between the amplitude of the inner surface temperature and that of outer surface temperature (Balaji et al., 2013).

The improvement of the thermal performance of building envelopes can be performed by using different strategies, such as: (*i*) improving the thermal transmittance coefficient or U-value; (*ii*) increasing the thermal mass or thermal inertia; and (*iii*) correcting thermal bridges. To improve the thermal transmission of a wall it is necessary to increase the wall's total resistance and normally it is reached by using thermal insulation material inside the walls. Thermal insulation is a material or combination of materials that because its low thermal conductivity, when properly applied, can significantly reduce the heat flow through it. The lower is a material thermal conductivity, more effective it is as an insulator.

Thermal inertia can be described as a rate of slowness which the temperature of a body tends to approach that of its surroundings. In the building envelope thermal aspects, thermal inertia is responsible of the reduction of the inside air temperature peaks and for the delay between the accumulation energy and its respective release and depends on two factors: (*i*) time lag and (*ii*) decrement factor. It also is influenced by the thermo-physical properties of the material, its thickness and position inside the wall (Bellahcene et al., 2017).

Thermal bridge is a definition of an area in an object which has higher thermal conductivity than the surrounding materials, resulting in a path with low resistance for heat transfer, creating a fast track for heat into or out the conditioned space through the wall. Their effects reduce the thermal resistance of building envelope and penalize the thermal behaviour and the energy efficiency of the building.

2.3 Light Steel Frame Construction

Lightweight steel frame (LSF) construction is a dry construction system characterized by the use of cold-formed steel profiles to build pre-fabricated panels or to be assembled directly on site. This construction system has emerged as a viable alternative to the traditional construction mostly because of its great advantages against the conventional concrete structure and masonry brick system, such as: (*i*) fast assemble, (*ii*) lightweight , (*iii*) high mechanical strength, (*iv*) better quality, (*v*) high architectural flexibility, (*vi*) suitable for mass production, (*vii*) great potential for recycling and reuse, (*viii*) less on-site waste, (*ix*) insect damage resistance, among others. (Soares et al., 2017).

A basic LSF wall is composed by three parts: (*i*) steel frame internal structure (cold formed profiles), (*ii*) sheathing panels (internal and exterior layers), and (*iii*) the cavity insulation material that could be filled with an insulation material, or empty. External LSF wall normally have the exterior thermal insulation composite system (ETICS), which is an exterior continuous insulations layer.

The existence of an insulation layer and its position on the wall determines the type of wall frame the LSF construction element has. According to Santos et al. (P. Santos et al., 2012), a LSF construction element can be classified into three wall frame typology, depending on the position of the thermal insulation on the wall, they are: (*i*) cold frame, (*ii*) warm frame and (*iii*) hybrid frame.

On cold frame constructions, the thermal insulation is placed inside the wall air cavity, between the vertical studs and limited to the stud depth. It is a non-continuous insulation layer, as it is crossed by the vertical studs, resulting on the worst thermal performance among the three constructions types, as the absence of an exterior insulation layer can cause low temperatures inside the wall especially around the steel stud area.

The opposite happens on the warm frame construction, where the totality of thermal insulation is continuous and located outside of the steel frame, isolating the exterior low temperatures and resulting on a frame temperature closer to the interior temperatures. This typology of construction has the best thermal insulation performance.

The hybrid construction type is an intermediate solution between cold and warm construction and has both type of insulation applied: outside and between the wall frame. As the outside continuous insulation, used on warm frame type, are more efficient, the greater thickness and quality of the outside insulation, better will be the thermal performance of the wall.

However, the LSF also may present some weaknesses, most of them related with the high thermal conductivity of the steel and the low thermal mass of the LSF elements, which could result on a poor thermal performance of the building. The low thermal inertia caused by the lower thermal mass on LSF constructions could affect the comfort inside dwellings, resulting on overheating problems during summer, large temperature fluctuations and higher energy demands for heating and cooling (Kendrick et al., 2012).

2.4 Thermal Performance of LSF Elements

The LSF constructions is characterized by the presence of an internal steel framing, made of highly conductive members spaced along the wall and interrupting the internal insulation layer. This causes a higher rate of heat transfer conduction through the wall framing than through other parts of the wall, which is called thermal bridges (Kosny et al., 1994).

Thermal bridges are fast heat path through the metallic structure and tend to increase heat losses though the wall. Their effects reduce the thermal resistance of the walls punishing the thermal behaviour and the energy efficiency of the building. Thermal bridges can also cause constructive pathologies reducing levels of comfort and healthy conditions related with the occurrence of condensation phenomena (Martins et al., 2016). To minimize the problems caused by thermal bridges, attenuation measures to mitigate their effect must be considered on the design phase.

Some building design strategies for improving the thermal resistance of LSF elements and mitigating the thermal bridges effects are: (*i*) keep the facade geometry as simples as possible, (*ii*) avoid the interruption on the insulation layer, (*iii*) join the insulation layer at full width at junctions of building elements, (*iv*) use insulation material with the lowest possible thermal conductivity whenever the interruption of the insulation layer were unavoidable and (*v*) install openings, such as doors and windows, in contact with the insulation layer (P. Santos et al., 2012).

Given the high level of heterogeneity regarding the thermal conductivities of the materials composing the LSF elements (steel frame and the thermal insulation), it is very challenging not only to accurately compute its thermal transmittance, but also to perform accurate and reliable measurements, both *in-situ* and in laboratory, especially when the steel profiles are placed in more than one direction. (Soares et al., 2019). When there is a thermal bridge, the flow of heat through the element becomes two-dimensional or even three-dimensional, rather than only in one-dimensional. The three-dimensional effect becomes more relevant due to the lateral heat flow originated by steel profiles. Therefore, some simplified methods should not be applied because, in theory, they may give imprecise results.

As will be later explained, the standard ISO 6946 (ISO 6946, 2017) describe the Combined Method, applicable for building elements containing homogenous and inhomogeneous layers, including the effect of metal fasteners, by means of a U-value correction term. However, this methodology is not applicable for LSF elements, where the thermal insulation is bridged by metal, as in cold and hybrid LSF construction.

Since the Combined Method is not applicable, in theory, for LSF elements where the thermal insulation is bridged by the steel frames, some researchers developed some alternative analytical methods for this type of structures. Gorgolewski (Gorgolewski, 2007) developed a simplified analytical method for calculating U-values in LSF cold and hybrid construction. This method was based in the principles provided by ISO 6946, but adapted to consider the increased thermal effect of the steel frame, increasing the accuracy of the proposed methodology.

Like the methods proposed by Gorgolewski, the ASHRAE (American Society of Heating, Refrigerating and Air-Conditioning Engineers) developed two methods (Zone Method and Modified Zone Method) to be used on constructions containing inhomogeneous layers like LSF constructions. As some of the previous described methods (*e.g.*, parallel path method) assumed that the heat flow is only perpendicular to the wall, when the wall structure contains steel framing members next to materials with low thermal conductivity, the two-dimensional effects

caused by thermal bridges become more relevant (Kosny et al., 1994). Both methods consider the lateral effect caused by metal studs on the calculation of the U-value.

Regarding the experimental approach there are several methods for the thermal characterization of building elements. For LSF elements the most suitable experimental method, given its large heterogeneity in its component materials thermal conductivity (*e.g.* steel and thermal insulation), is the hot box apparatus, since the measurements are not local, but instead in a representative wall area (ISO 8990, 1994).

On the following sections 2.6.2 and 2.6.3 will be presented two methodologies specially developed to evaluate the thermal transmittance of LSF walls (Gorgolewski, 2007) (ASHRAE, 2017).

2.5 Thermal Transmission of a Construction Element

The thermal transmittance (U-value) of an opaque building element depends on several factors, such as the thickness of each layer, the number of layers, the thermal conductivity (λ) of each layer material, the existence of thermal bridges due to the presence of an inhomogeneous thermal layer, the existence of air voids in the insulation, the external and internal surface thermal resistances (ISO 6946, 2017).

In a steady-state perspective, the thermal performances of building elements depend on the thermal conductivity (λ) of each layer of the wall – which gives information about how heat flows through a structure – and the heat capacity (c_p) of the layers – which is related to material heat storage. The thermal resistance (R) is inversely related with the thermal conductivity, it means that higher thermal resistance values are obtained with lower thermal conductivity (λ) values. The thermal transmittance coefficient, namely the U-value, is used to quantify the overall heat exchange between interior and exterior environment through a building envelope (Asdrubali et al., 2015).

However, the layer-by-layer approach to determine the thermal transmittance of a wall does not take into consideration the effects of thermal bridges, air gaps around insulation, cavities with air movements, moisture contents, and others details that prejudice the thermal performance of a construction element. Thermal bridges are characterized by a variation in the heat flow with a consequent lowering of internal surfaces temperatures (ISO 10211, 2017) which can promote mold and other pathologies caused by condensation.

There are different ways to calculate the U-value for a construction element: analytical approach, numerical simulation and experimental evaluation. On the next sub-sections will be briefly introduced the numerical simulations and the experimental evaluation as methods to calculate the U-value. The analytical methods to evaluate the thermal transmittance of a construction element will be explained on Section 2.6.

2.5.1 Numerical Simulation

Several numerical computational methods are available to reproduce highly detailed models of building components providing accurate and reliable values for their thermal properties and thermal behaviour under any kind of pre-established condition. The numerical methods can be classified can be classified as one-dimensional (1D), two-dimensional (2D) or three dimensional (3D).

2.5.2 Experimental Evaluation

The experimental evaluations for construction elements are very important procedures to validate the numerical and analytical models and to calculate the thermal transmittance of more complex configurations structures. Those experimental evaluations can be performed in laboratory – where the environment conditions are simulated by laboratory's equipment – or can be performed directly *in-situ*, *i.e.* where the element is built. The non-destructive *in-situ* measurements to determine the overall thermal transmittance of existing walls are very useful procedures to energy auditions and building's retrofitting (ISO 9869-1, 2014).

Some examples of experimental evaluation methodologies are: (*i*) the heat flow meter (HFM), (*ii*) the guarded hot plate (GHP), (*iii*) the guarded hot box (GHB), (*iv*) the calibrated hot box (CHB) and, (*v*) the infrared thermography (IRT).

2.6 Analytical Calculation Methods

There are some analytical methods to estimate walls U-value and R-value, most of them uses the materials thermal properties (*e.g.* thermal conductivity) to get a resistance value for each material layer. For building elements formed by only homogeneous layers, calculating the total thermal resistance (R_{tot}) is just compute the layers resistances summation and using the simplified method to find the wall transmittance, as shown on Equation (1).

$$U = {}^{1}/_{R_{tot}} \tag{1}$$

However, most of the building constructions contain inhomogeneous walls, which makes it difficult to estimate thermal transmittance values with simple methodology. When a building element is constituted by n homogeneous layers (j), perpendicular to the heat flow, the originated heat flow transfer is one-dimensional and the total thermal resistance (environment to environment) could be computed as prescribed by ISO 6946 (ISO 6946, 2017),

$$R_{\text{tot}} = R_{\text{si}} + \sum_{j=1}^{n} R_j + R_{\text{se}} \tag{2}$$

where R_{si} and R_{se} are the internal and external surface resistances and R_j is the thermal resistance of each homogeneous layer j.

When there are inhomogeneous layers in the building component, the heat flow starts being two-dimensional, instead of only one-dimensional, given to the different thermal conductivities' values and consequent different thermal resistances. These two-dimensional heat flow features get stronger when the discrepancies between the thermal properties of the materials, within the same layer, are more significant.

2.6.1 ISO 6946 Combined Method

The analytical method described on ISO 6946 (ISO 6946, 2017) is one of the most used method to compute the thermal resistance of building elements consisting of thermally homogeneous and inhomogeneous layers, which may contain air layers up to 0.30 m thick, being also often referred as ISO 6946 Combined Method. The reference as "combined method" comes from the total thermal resistance (R_{tot}) calculation process, which is reached making use of two different methods to calculate the partials thermal resistances $R_{tot;lower}$ and $R_{tot;upper}$: the Parallel Path Method and the Isothermal Planes Method.

The total thermal resistance ($R_{\text{tot;ISO}}$) is computed as an arithmetic average of the total upper ($R_{\text{tot;upper}}$) and lower ($R_{\text{tot;lower}}$) limits of thermal resistances,

$$R_{\text{tot;ISO}} = \frac{R_{\text{tot;upper}} + R_{\text{tot;lower}}}{2} \tag{3}$$

which means that the both partial resistances (upper and lower) have the same weight (0.5 for each) on the total resistance calculation (ISO 6946, 2017).

Although, according to ISO 6946 (ISO 6946, 2017), this simplified analytical approach is only valid for the cases where the ratio of the upper limit ($R_{tot;upper}$) to the lower limit ($R_{tot;lower}$) of the thermal resistances is lower than 1.5. Moreover, this method is not applicable to building elements where thermal insulation is bridged by metal (*e.g.* steel studs), *i.e.* when there is a significant difference between the thermal conductivity (λ) of the materials in the layer providing the most important thermal resistance of the building element.

After calculating the total thermal resistances ($R_{\mathrm{tot;ISO}}$), to estimate the total thermal transmittance (U) for the wall element through Equation (4),

$$U = \frac{1}{R_{tot;ISO}} + \Delta U \tag{4}$$

where ΔU is the correction terms for relevant effects.

Those relevant effects are: air gaps insulation (ΔU_g), mechanical fasteners penetration an insulation layer (ΔU_f) and precipitation on inverted roofs (ΔU_r), and they are related as indicated the Equation (5).

$$\Delta U = \Delta U_g + \Delta U_f + \Delta U_r \tag{5}$$

2.6.1.1 Upper Limit of the Total Thermal Resistance: Parallel Path Method

The upper limit of the total thermal resistance ($R_{\mathrm{tot;upper}}$) is determined making use of the parallel path method, *i.e.*, assuming one-dimensional heat transfer perpendicular to the surfaces of the building element where the heat is transferred exclusively in this direction. This method is normally used when the materials on the same layer have close ($i.e.$, same order of magnitude) thermal conductivity values, as for example, on wood frame walls.
As illustrated in Figure 2.1, the wall cross-section is divided into two sections, A and B, each one with a different heat path in parallel, and with different resultant thermal resistances values.

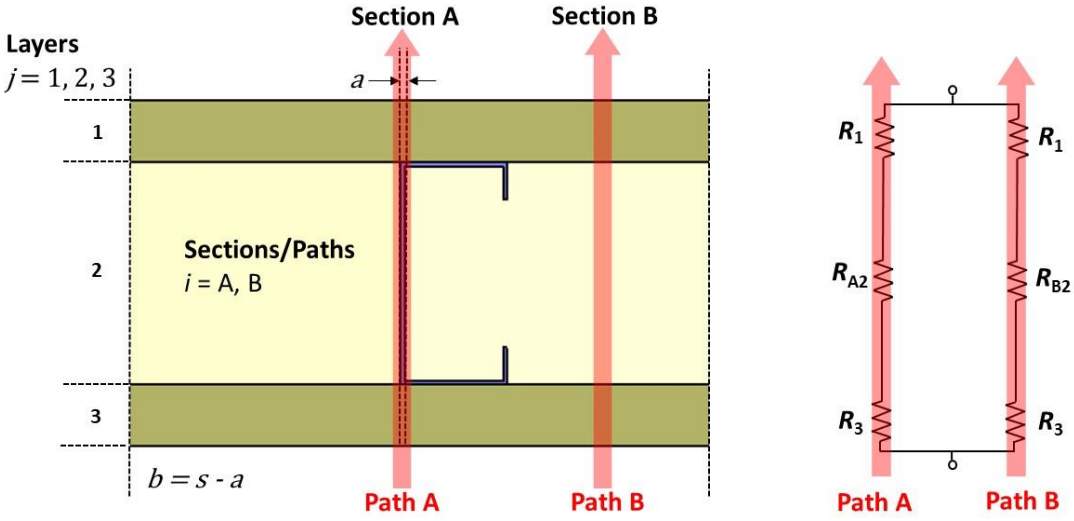

(a) (b)

Figure 2.1 – Parallel Path Method schematic illustration: (a) LSF wall cross-section; (b) Equivalent series-parallel circuit (P. Santos et al., 2020).

Section A comprises the location of the highly conductivity material (steel stud) and where the heat flux will be higher. Section B represents the remaining part of the wall cross-section area and where the heat flux is lower, given by the lower thermal conductivity values from the cavity insulation material.

The heat flow of each path (A and B) are assumed to be independent from each other and its path's thermal resistance ($R_{tot;A}$ and $R_{tot;B}$) are calculated using a series circuit relationship analogous to electrical resistances as displayed on Figure 2.1b, *i.e.*, they are computed as the summation of the layers' resistances, using Equation (2) (ISO 6946, 2017).

Similarly to what occurs in electrical circuits, the equivalent thermal resistance (R_j) of the thermally inhomogeneous layer (j), represented as two or more thermal resistances in parallel, is computed using the parallel path method according to the generic Equation (6),

$$\frac{1}{R_j} = \frac{f_A}{R_{Aj}} + \frac{f_B}{R_{Bj}} + \cdots + \frac{f_Q}{R_{Qj}} \tag{6}$$

where $f_A, f_B, \ldots, f_Q$ are the fraction areas of the wall's sections.

Then, the upper limit of the total thermal resistance ($R_{\mathrm{tot;upper}}$) is calculated as a parallel circuit between the equivalent thermal resistances from path A ($R_{tot;A}$) and path B ($R_{tot;B}$) by using the generic Equation (6), that could be simplified for the LSF wall illustrated in Figure 2.1, resulting on Equation (7).

$$\frac{1}{R_{\mathrm{tot;upper}}} = \frac{f_{\mathrm{A}}}{R_{\mathrm{tot;A}}} + \frac{f_{\mathrm{B}}}{R_{\mathrm{tot;B}}} \tag{7}$$

where f_{A} and f_{B} are the fractional areas of sections A and B.

This methodology does not consider the steel stud flanges (horizontal parts) and stud returns (vertical small part), only considering the web of the stud, which thickness delimits the width of Section A.

2.6.1.2 Lower Limit of the Total Thermal Resistance: Isothermal Planes Method

The lower limit of the total thermal resistance ($R_{\mathrm{tot;lower}}$) is calculated making use of the isothermal planes method. In this method, assuming the heat flow is perpendicular to the wall, the heat can flow laterally through components, creating planes, parallel to wall surface, with the same temperature, *i. e.* isothermal planes. It is the most appropriate method when adjacent materials of the same layer have conductivity values moderately different, as with masonry walls (ASHRAE, 2017).

On inhomogeneous layers, the resistances of the adjacent materials are combined in parallel, resulting on a path with series-parallel resistances combined (Kosny et al., 1994). The Figure 2.2a illustrates an LSF wall cross-section where layer 2 is an inhomogeneous layer (insulation material and steel stud), enabling two possible paths for the heat flows (through section A and B) creating a parallel system between two different thermal resistances (R_{A2} and R_{B2}). The equivalent series-parallel circuit for this wall is shown on Figure 2.2b. Due to the insulation material placed on the cavity, the thermal resistance of section B (R_{B2}) is greater than section A (R_{A2}). As in the previously method (parallel path), only the web of the steel stud is considered for heat transfer calculation purposes.

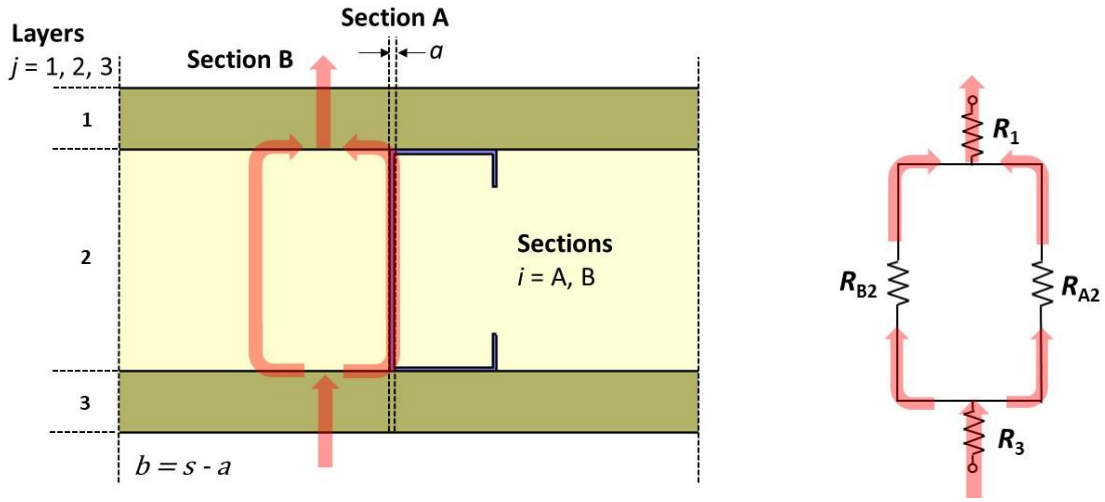

(a) (b)

Figure 2.2 – Isothermal planes method schematic illustration: (a) LSF wall cross-section; (b) equivalent series-parallel circuit.

To calculate the lower limit of the total thermal resistance ($R_{\text{tot;lower}}$), first is necessary to compute the equivalent thermal resistance (R_j) of the thermally inhomogeneous layers (j), using the parallel path method according to Equation (6), which can be simplified for the LSF wall illustrated in Figure 2.2, resulting on Equation (8).

$$\frac{1}{R_2} = \frac{f_{\text{A}}}{R_{\text{A2}}} + \frac{f_{\text{B}}}{R_{\text{B2}}} \tag{8}$$

After calculating the equivalent thermal resistant from every inhomogeneous layer, the lower limit of the total thermal resistance ($R_{\text{tot;lower}}$) is computed as the summation of the layers' resistances, as an analogous series circuit relationship using Equation (2). For the wall configuration from Figure 2.2, after the simplification, results on Equation (9).

$$R_{\text{tot;lower}} = R_{\text{si}} + R_1 + R_2 + R_3 + R_{\text{se}} \tag{9}$$

2.6.2 Gorgolewski Methods

As previously explained in Section 2.6.1, the ISO 6946 Combined Method U-value calculation excludes from its scope wall's configurations in which insulating layers are bridged by linear metal elements, like on lightweight steel frame (LSF) construction. Gorgolewski (Gorgolewski, 2007) has proposed three new methods based on similar principles used in that standard (ISO 6946, 2017), adapting it to increase the accuracy for this type of construction. Using the same calculation methodology proposed on ISO 6946 to reach upper ($R_{\mathrm{tot;upper}}$) and lower ($R_{\mathrm{tot;lower}}$) limits of the thermal resistances, Gorgolewski methods differs at the total resistance calculation by applying different weights for upper and lower resistance values when considering a factor p, between 0 and 1, such that the total thermal resistance (R_{tot}) is given by Equation (10),

$$R_{\mathrm{tot;gorg}} = p\, R_{\mathrm{tot;upper}} + (1-p)\, R_{\mathrm{tot;lower}} \tag{10}$$

For warm frame LSF elements, $i.e.$, when there is only external insulation, it was assumed a p-value equal to 0.5 (Doran & Gorgolewski, 2002). Thus, the obtained total thermal resistance for any of the Gorgolewski methods is equal to the one provided by ISO 6946 Combined Method. In his work, Gorgolewski (Gorgolewski, 2007) verified the calculation methods by comparing it to the results provided by two-dimensional (2D) finite element method (FEM) models for 52 different LSF walls and roof slabs.

2.6.2.1 Method 1

After his firsts comparison work, Gorgolewski has refined the accuracy of the calculation results, proposing the Method 1 in which the p-value is calculated by Equation (11).

$$p = 0.8\left(\frac{R_{tot;lower}}{R_{tot;upper}}\right) + 1 \tag{11}$$

This p-value depends directly on the ratio between the lower and upper limits of the total thermal resistance.

2.6.2.2 Method 2

For the second method, Gorgolewski took into consideration the LSF wall frame type, whether it is the hybrid or cold one. For this, it was proposed the Table 2.1 that also considers the stud spacing.

Table 2.1 – Tabulated p-values for Gorgolewski Method 2 (Gorgolewski, 2007).

p-values	Frame type	
	Hybrid	**Cold**
Stud spacing ≥ 500 mm	0.50	0.30
Stud spacing < 500 mm	0.40	0.25

2.6.2.3 Method 3

Combining the previous approaches, Gorgolewski (Gorgolewski, 2007) developed the third method by including additional terms, whose accounts for the overall behaviour of the steel frame designs, on Equation (12):

$$p = 0.8\left(\frac{R_{\text{tot;lower}}}{R_{\text{tot;upper}}}\right) + 0.44 - 0.1\left(\frac{L}{0.04}\right) - 0.2\left(\frac{0.6}{s}\right) - 0.04\left(\frac{sd}{0.1}\right) \quad (12)$$

Apart of the dependence of the ratio between the lower and upper limits of the total thermal resistance and the constant 0.44 parcel, there are three more variables, very particular from LSF walls, that have influence on p-value and were included in this method's equation, there are: flange width (L), stud spacing (s) and stud depth (sd), being all these dimension expresses in meters.

2.6.3 ASHRAE Methods

The ASHRAE methods were developed for structures with widely spaced metal members of substantial cross-sectional areas and when the adjacent materials have very high different conductivities (two order or more of magnitude), as what happens on typical LSF constructions where metal parts and thermal insulation materials are placed side by side (ASHRAE, 2017).

Those two methods (Zone and Modified Zone Methods) are an adjustment of the parallel path method, where some factors that increase the heat path were added to calculation of the width of the wall sections. These factors are related to the thermal bridges caused by highly conductivity elements of the wall influencing a larger area around them (Kosny et al., 1994).

As show on Figure 2.3, the section W represents the area containing the metal stud and its thermal bridge influence area. The remaining portion of the wall, a simpler part composed only by homogeneous layers is called section CAV.

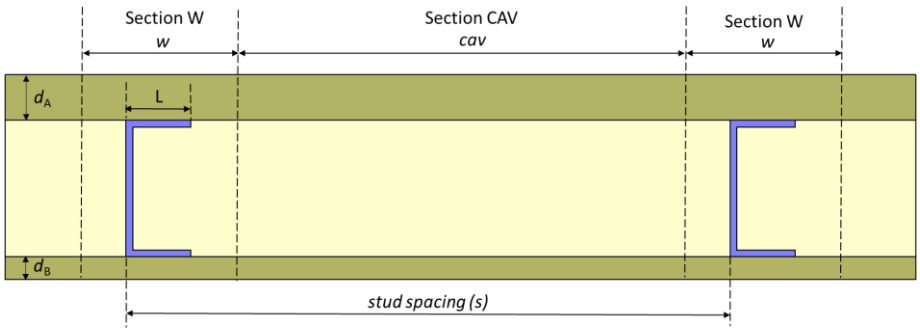

Figure 2.3 – LSF wall cross-section illustration for the ASHRAE methods: section W and CAV (ASHRAE, 2017).

The section W is centered on the metal part and its length, w, is determined by Equation (13),

$$w = L + zf \cdot d_A \tag{13}$$

where: L is the flange length, zf is the zone factor and d_A is the thickness of the thicker sheathing side (interior or exterior).

For both sections paths, the thermal resistances values are computed and them combined using the parallel path method and the average thermal transmittance per unit overall area (U-value) is calculated by reversing the total thermal resistance, $U = 1/R_{tot}$.

2.6.3.1 Zone Method

The first method proposed by ASHRAE, the Zone Method, uses Equation (13) to calculate the length of section W, however, for this method, the zone factor, zf, is equal to 2.0. The

remaining calculations for both ASHRAE methods, the total thermal resistance (R_{tot}) and transmittance (U), are the same and will be presented next.

The detailed dimension of Section W is illustrated in Figure 2.4a. Moreover, the equivalent series-parallel circuit used in the simplified heat transfer calculations is displayed in Figure 2.4b. For calculation purposes, the metal C-stud shape was simplified and considering only the web and both flanges, being neglected the return part.

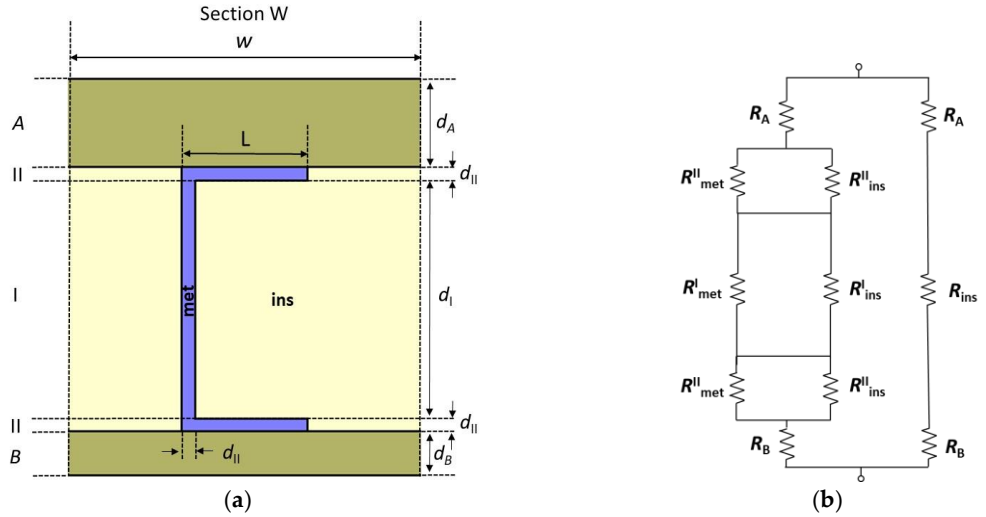

Figure 2.4 – ASHRAE methods section W detailed: (a) LSF cross-section layers and interstitial layers (I and II); (b) Equivalent series-parallel circuit (ASHRAE, 2017) (Kosny et al., 1994).

The total thermal resistance, R_{tot}, of a generic LSF wall is computed applying the parallel path method to both sections W and CAV according Equation (14),

$$\frac{1}{R_{\mathrm{tot;ASHRAE}}} = \sum_{i=1}^{2} \frac{f_i}{R_i} = \frac{w/s}{R_{\mathrm{tot;W}}} + \frac{cav/s}{R_{\mathrm{tot;CAV}}} \tag{14}$$

where: $R_{\mathrm{tot;W}}$ and $R_{\mathrm{tot;CAV}}$ are the total thermal resistances [m^2. K/W] of sections W and CAV, respectively; w and cav are the lengths [m] of sections W and CAV, respectively; and s is the studs spacing [m].

The total thermal resistance of the homogeneous layers of the LSF wall cavity, $R_{\mathrm{tot;CAV}}$, is computed as the summation of all layer's thermal resistances in series, including the internal and external surface thermal resistances,

$$R_{\mathrm{tot;CAV}} = R_{\mathrm{si}} + R_{\mathrm{A}} + R_{\mathrm{ins}} + R_{\mathrm{B}} + R_{\mathrm{se}} \quad (15)$$

where: R_{ins} is the thermal resistance of the entire insulation layer $[(\mathrm{m}^2.\mathrm{K})/\mathrm{W}]$.

The total thermal resistance of the Section W, $R_{\mathrm{tot;W}}$, is computed making use of the isothermal planes method. First, the equivalent thermal resistance (R_j) of each thermally inhomogeneous layer, interstitial layers I and II, are calculated making use of the parallel path method to both metal (met) and insulation (ins) paths,

$$\frac{1}{R_{\mathrm{II}}} = \frac{L/w}{R_{met}^{\mathrm{II}}} + \frac{(w-L)/w}{R_{ins}^{\mathrm{II}}} \quad (16)$$

$$\frac{1}{R_{\mathrm{I}}} = \frac{d_{\mathrm{II}}/w}{R_{met}^{\mathrm{I}}} + \frac{(w-d_{\mathrm{II}})/w}{R_{ins}^{\mathrm{I}}} \quad (17)$$

where the partial resistances R_{met}^{II}, R_{ins}^{II}, R_{met}^{I} and R_{ins}^{I} can be defined dividing its thickness (d) to its thermal conductivity value (λ), *i.e.* $R = \mathrm{d}/\lambda$.

After this, the equivalent thermal resistances are used to compute the total thermal resistance of the Section W, having into account all partial thermal resistances as well as the surface thermal resistances, using the Equation (18).

$$R_{\mathrm{tot;W}} = R_{\mathrm{si}} + R_A + R_B + R_I + 2R_{II} + R_{\mathrm{se}} \quad (18)$$

2.6.3.2 Modified Zone Method

The Modified Zone Method is very similar to the Zone Method, making use of the same equations (Equations (14) to (18)) to reach the partials and total thermal resistances, being the only difference between them the definition of the width (w) for section W. The Modified Zone Method uses a modified zone factor (zf) value, which is not a constant and not necessarily equal to 2. For this method, the width (w) of the steel stud influence zone (section W), besides the flange length (L), depends on other three parameters (ASHRAE, 2017): (i) the ratio between

thermal resistivities of sheathing material and cavity insulation material; (*ii*) the size (depth) of stud; and (*iii*) the thickness of the sheathing material.

To determine the zone factor (z_f) is necessary to know the resistivity (r) of exterior sheathing material and of the cavity insulation material. The resistivity (r) of a material is the reciprocal of thermal conductivity (λ), *i.e.*, $r = 1/\lambda$. The ratio between the resistivity of the external sheathing material (r_{sheat}) and cavity insulation material (r_{ins}), combined with the stud size, will be used to find the zone factor (z_f) on the chart presented on Figure 2.5.

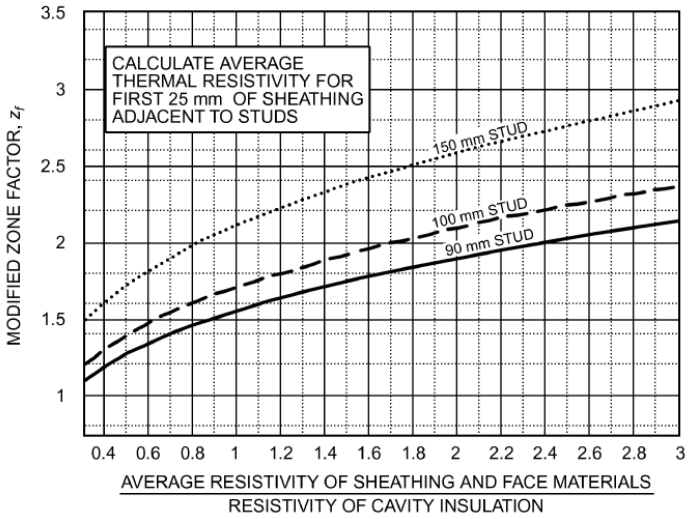

Figure 2.5 – Modified zone factor (zf) for metal stud walls with cavity insulation (ASHRAE, 2017).

To calculate the ratio between the materials' resistivities, must be taken into account the average resistivity for the first 25 mm of the external sheathing material adjacent to the studs (r_{sheat}) and then, dividing it by the resistivity of the cavity insulation material (r_{ins}).

The condition for using the chart presented on Figure 2.5 is that for at least one of the sides of the wall, the total thickness of layers must be thicker than 16 mm. If both sides of the wall have the total thickness smaller than 16 mm, the z_f values should be used according to the conditions explained on Figure 2.6.

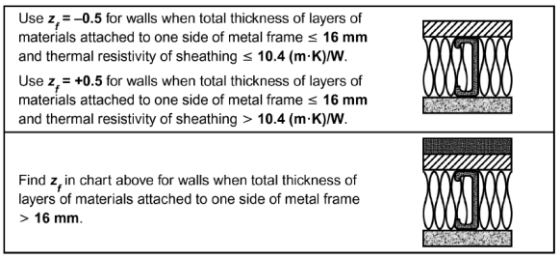

Figure 2.6 – Conditions for zone factor (zf) determination (ASHRAE, 2017).

3 A PARAMETRIC STUDY WITH INTERIOR AND EXTERIOR LSF WALLS

In this chapter a parametric study was performed using numerical simulations to assess two kinds of LSF walls: an interior partition and an exterior facade. Several parameters were evaluated separately to measure their influence on the wall U-value and comparing with the results of its reference wall. It was also evaluated the addition of thermal break strips made with different materials, with the aim to reach better thermal performances. This work was subject of the paper "Thermal Transmittance of Internal Partition and External Facade LSF Walls: A Parametric Study" (P. Santos et al., 2019).

3.1 LSF Wall Characterization

To evaluate the influence of each parameter on the thermal behaviour of LSF walls it is first necessary to define the configuration of each reference model. In the next sub-sections will be characterized the configurations of the LSF interior partition and exterior facade reference walls.

3.1.1 Interior Reference Wall and Evaluated Parameters

The interior partition reference wall is a configuration of LSF normally used as an internal partition within the same dwelling. As illustrated on Figure 3.1, this LSF internal partition is constituted by two gypsum plasterboards (12.5 mm thick each) on each side of the steel frame (made with steel studs C90, 90 mm wide, and 0.6 mm of steel sheet thickness) and the air cavity is fully filled with mineral wool batt insulation (90 mm). The distance between vertical profiles for internal reference walls was set on 600 mm. The total thickness of this partition wall is 140 mm.

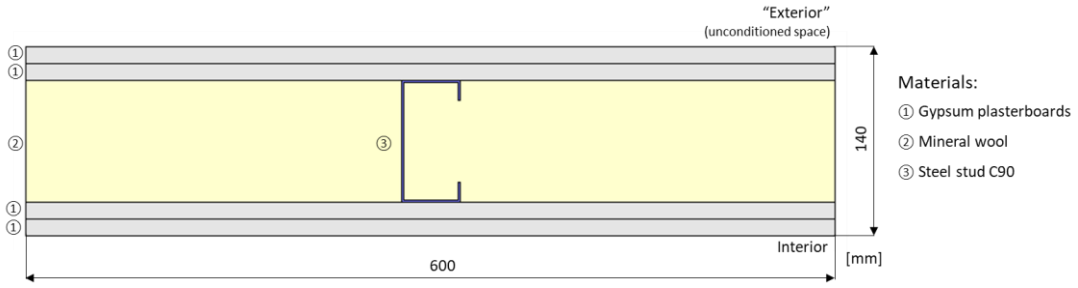

Figure 3.1 – Cross-section of an interior LSF reference wall (P. Santos et al., 2019).

Even being an internal partition, this LSF wall can separate a conditioned space from an unconditioned space, *e.g.* a garage, with lower temperature. Therefore, this internal partition has also thermal requirements. Table 3.1 also displays the thickness (d) of each material layer, as well as the thermal conductivity (λ) of each material.

Table 3.1 – Material characteristics of the interior LSF reference wall (P. Santos et al., 2019).

Layer	**Material** (from "outer" to innermost layer)	$\boldsymbol{d}$ [mm]	$\boldsymbol{\lambda}$ [W/(m.K)]	**References**
1	GPB[1] (2 × 12.5 mm)	25	0.175	(Gyptec Ibérica, 2019)
2	Mineral wool	90	0.035	(Volcalis, 2019)
3	Steel stud (C90 × 43 × 15 × 0.6 mm)	90	50.000	(C. Santos & Matias, 2006)
4	GPB (2 × 12.5 mm)	25	0.175	(Gyptec Ibérica, 2019)
	Total Thickness	140	---	

[1] GPB – Gypsum Plaster Board.

As from the interior reference wall other walls configurations were created, in which one parameter has been modified at a time and identified as a different wall model. Table 3.2 displays the wall models and its correspondent parameter evaluated on the sensitivity analyses, as well as the reference value (reference wall) and the other three varied values.

Table 3.2 – Interior partition LSF wall models and parameters evaluated values (P. Santos et al., 2019).

Wall Model	Evaluated Parameter	Ref. Value	Value 1	Value 2	Value 3
I1	**Thickness of Steel Studs** [mm]	0.6	1.0	1.2	1.5
I2	**Clearance Between Steel Studs** [mm]	600	300	400	800
I3	**Thickness of Aerogel TB[1] Strips** [mm]	0.0	2.5	5.0	10.0
I4	**Material of TB[1] Strips with 10 mm**	---	MS-R1[2]	XPS[3]	CBS[4]
I5	**Sheathing Panels Materials**				
	GPB[5] Thickness [mm]	2×12.5	12.5	---	12.5
	OSB[6] Thickness [mm]	---	12.0	2×12.0	---
	XPS[3] Thickness [mm]	---	---	---	12.0

[1]TB – Thermal Break; [2]MS-R1 – Acousticork (recycled rubber); [3]XPS – Extruded Polystyrene; [4]CBS – Cold Break Strip (aerogel); [5]GPB – Gypsum Plaster Board; [6]OSB – Oriented Strand Board.

The parameters evaluated in each wall model are: (I1) the thickness of the steel studs; (I2) the stud spacing; (I3) the material and thickness of the thermal break (TB) strips; (I4) the TB strip materials and (I5) the sheathing panels materials. The wall models' configurations are illustrated on Figure 3.2.

The first parameter evaluated was the thickness of the steel sheet used to conform the studs for the wall steel frame and are represented on the wall models I1, where the reference value is 0.6 mm, a usual value for non-load-bearing partition wall. It has been also modelled steel profiles with 1.0 mm, 1.2 mm and 1.5 mm thick, as it is displayed in Table 3.2 and illustrated in Figure 3.2a. The amount of steel inside the wall structure is very relevant because metal has a very high thermal conductivity and its presence in LSF frames create a path that allow the heat to easily cross through the walls, as steel thermal bridges.

The wall models I2 evaluated the parameter of the distance between vertical studs in order to assess its relevance on the thermal behaviour of the LSF internal walls. The reference wall has a distance of 600 mm between steel studs (Figure 3.1) and three more distances were evaluated: 300 mm, 400 mm and 800 mm (Figure 3.2a).

As a strategy to mitigate the heat loss through the thermal bridges causes by the steel structure and to improve the thermal transmittance (U-value) of the LSF walls, could be the insertion of an insulation material between the steel structure and its adjacent layer, working as a thermal

break. On the wall models I3 has been evaluated an aerogel thermal break strips in three different thickness: 2.5 mm, 5.0 mm and 10.0 mm (Figure 3.2b).

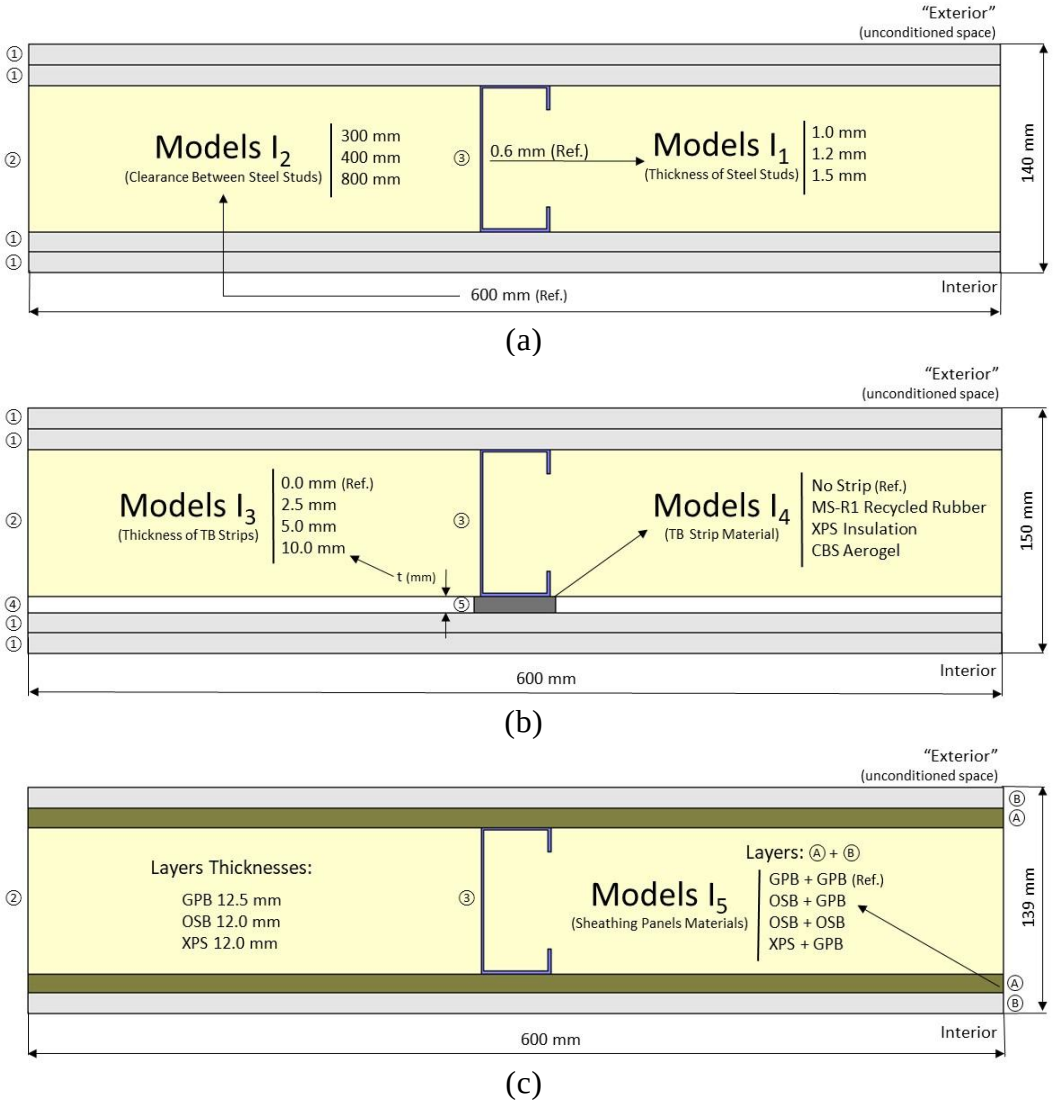

Figure 3.2 – Interior LSF partition wall models cross-sections: (a) I1 and I2; (b) I3 and I4; (c) I5. Layers: ① Gypsum plasterboard (GPB); ② Mineral wool; ③ Steel stud C90; ④ Air layer; ⑤ TB strip (P. Santos et al., 2019).

The parameters assessed on the wall models I4 were the insulation material used for the thermal breaks strips where three different materials were tested, such as: (*i*) recycled rubber (value 1), (*ii*) extruded polystyrene XPS (value 2) and (*iii*) aerogel (value 3). The thicknesses of the thermal breaks strips for this evaluation were of 10.0 mm and its thermal conductivities are listed on Table 3.3.

Table 3.3 – Thermal conductivities (λ) of thermal break strips materials (P. Santos et al., 2019).

Material	$\boldsymbol{\lambda}$ [W/(m.K)]	**Ref.**
Recycled Rubber (Acousticork MS-R1)	0.122	(MS-R1, 2017)
XPS[1] Insulation	0.037	(C. Santos & Matias, 2006)
CBS[2] Aerogel (Spacetherm)	0.015	(Spacetherm, 2018)

[1]XPS – Extruded Polystyrene; [2]CBS – Cold Break Strip.

The wall models I5 assessed the influence of the sheathing panels materials parameter, where several configurations of internal wall were modelled as shown on Table 3.2 and displayed in Figure 3.2c. For the reference wall, the sheathing panels are two gypsum plasterboard panels on each side of the steel structure. On the first parameter variation (value 1) the innermost gypsum plasterboard was replaced by one OSB panel (12.0 mm) in both sides of the LSF structure. For value 2, both gypsum plasterboards were replaced by two OSB panels on each side. Regarding the third variation (value 3), as in the first variation, the innermost gypsum plasterboard was replaced on both sides, but now by XPS panels with 12.0 mm thick each.

3.1.2 Exterior Reference Wall and Evaluated Parameters

The reference exterior wall is an LSF wall normally used for facades, which means that it is a wall that must be prepared to handle high gradients of environment temperature and often have to support load. Therefore, it has an extra thermal insulation layer which was placed on its outsider surface. In this case, it was chosen an ETICS (External Thermal Insulation Composite Systems) system using EPS (Expanded Polystyrene) as insulation main material (50 mm).

The steel structure that forms the wall frame is made of galvanized cold-formed vertical C90 studs and, different for internal walls, the thickness of the steel profile sheet is now 1.5 mm. Similarly to the interior LSF walls, the distance between vertical profiles for the reference wall is 600 mm. The horizontal cross-section that shows all the layers of the reference exterior LSF wall is illustrated in Figure 3.3 and the specifications and characteristics of internal composition materials are detailed in Table 3.4.

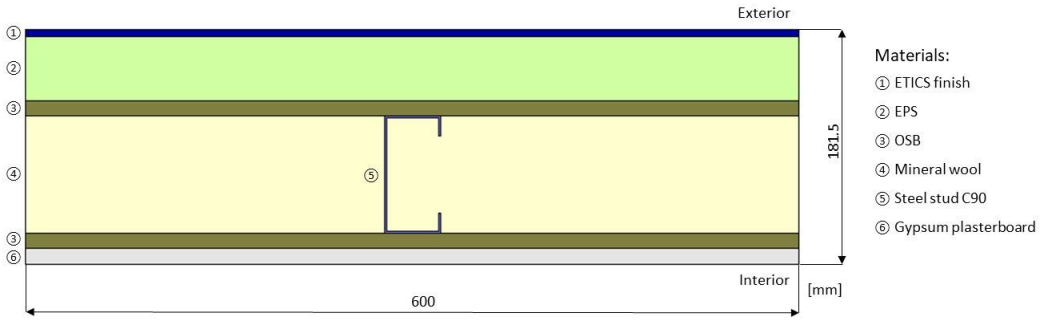

Figure 3.3 - Cross-section of an exterior LSF reference wall (P. Santos et al., 2019).

Table 3.4 - Material characteristics of the exterior LSF reference wall (P. Santos et al., 2019).

Layer	**Material** (from outer to innermost layer)	***d*** [mm]	**λ** [W/(m.K)]	**References**
1	ETICS[1] finish	5	0.450	(WeberTherm Uno, 2018)
2	EPS[2]	50	0.036	(TincoTerm, 2015)
3	OSB[3]	12	0.100	(KronoSpan, 2019)
4	Mineral wool	90	0.035	(Volcalis, 2019)
5	Steel stud (C90 × 43 × 15 × 1.5 mm)	90	50.000	(C. Santos & Matias, 2006)
6	OSB	12	0.100	(KronoSpan, 2019)
7	GPB[4]	12.5	0.175	(Gyptec Ibérica, 2019)
	Total Thickness	**181.5**	---	---

[1]ETICS - External Thermal Insulation Composite System; [2]EPS – Expanded Polystyrene; [3]OSB - Oriented Strand Board; [4]GPB - Gypsum Plaster Board.

Likewise to the interior partition wall, a parametric study was made for the LSF exterior facade walls based on the evaluations of different walls models where a parameter was modified at a time. The wall models, its correspondent evaluated parameters and variated values are displayed on Table 3.5 and illustrated in Figure 3.4.

Table 3.5 – Exterior facade LSF wall models and parameters evaluated values (P. Santos et al., 2019).

Wall Model	Evaluated Parameter	Ref. Value	Value 1	Value 2	Value 3
E1	**Thickness of Steel Studs** [mm]	1.5	0.6	1.0	1.2
E2	**Clearance Between Steel Studs** [mm]	600	300	400	800
E3	**Thickness of Aerogel TB[1] Strips** [mm]	0.0	2.5	5.0	10.0
E4	**Material of TB Strips with 10 mm**	---	MS-R1[2]	XPS[3]	CBS[4]
E5	**Inner Sheathing Panels Materials**				
	GPB[5] Thickness [mm]	12.5	---	2×12.5	12.5
	OSB[6] Thickness [mm]	12.0	2×12.0	---	---
	XPS[7] Thickness [mm]	---	---	---	12.0
E6	**Thickness of EPS[8] in ETICS[9]** [mm]	50	0.0	30	80

[1]TB – Thermal Break; [2]MS-R1 – Acousticork (recycled rubber); [3]XPS – Extruded Polystyrene; [4]CBS – Cold Break Strip (aerogel); [5]GPB – Gypsum Plaster Board; [6]OSB – Oriented Strand Board; [7]XPS – Extruded Polystyrene; [8]EPS – Expanded Polystyrene; [9]ETICS – External Thermal Insulation Composite System.

The thickness of steel studs used on LSF wall steel frame was the first parameter evaluated (models E1). The reference value for exterior wall is 1.5 mm and the three additional thicknesses assessed are: 0.6 mm, 1.0 mm, and 1.2 mm (Figure 3.4a). Regarding the distance between the vertical steel studs, this parameter was evaluated on the wall models E2. The reference exterior wall has 600 mm clearance and was also modelled the values of: 300 mm, 400 mm and 800 mm (Figure 3.4a). The same as for the interior partition walls, the thermal break strips thickness (models E3) and materials (models E4) assessments were performed the same way (Figure 3.4b).

To verify the influence of the internal sheathing panels (models E5), the exterior facade wall were tested in different configurations for the innermost layer, as shown on Table 3.5 and illustrated in Figure 3.4c. The reference exterior wall internal sheathing is composed by one OSB (12.0 mm) and one GPB (12.5 mm) panels, being the OSB panel very important in load bearing walls giving extra resistance to horizontal lateral loads (Henriques et al., 2017). For the first variation (value 1), the internal sheathing panels are composed by two OSB with 12.0 mm each. For the second variation (value 2), the internal layers are formed by two gypsum plasterboards (GPB) with 12.5 mm each. In the third variation (value 3) the OSB panel, adjacent to the steel stud, is replaced by one XPS panel with the same thickness (12.0 mm).

The influence of the ETICS insulation layer is evaluated on the models E6, where the parameter assessed is the thickness of the EPS insulation material. For the LSF exterior reference wall the thickness is 50 mm and three more values were also evaluated, they are: 0.0 mm (no EPS insulation), 30 mm and 80 mm (Figure 3.4c).

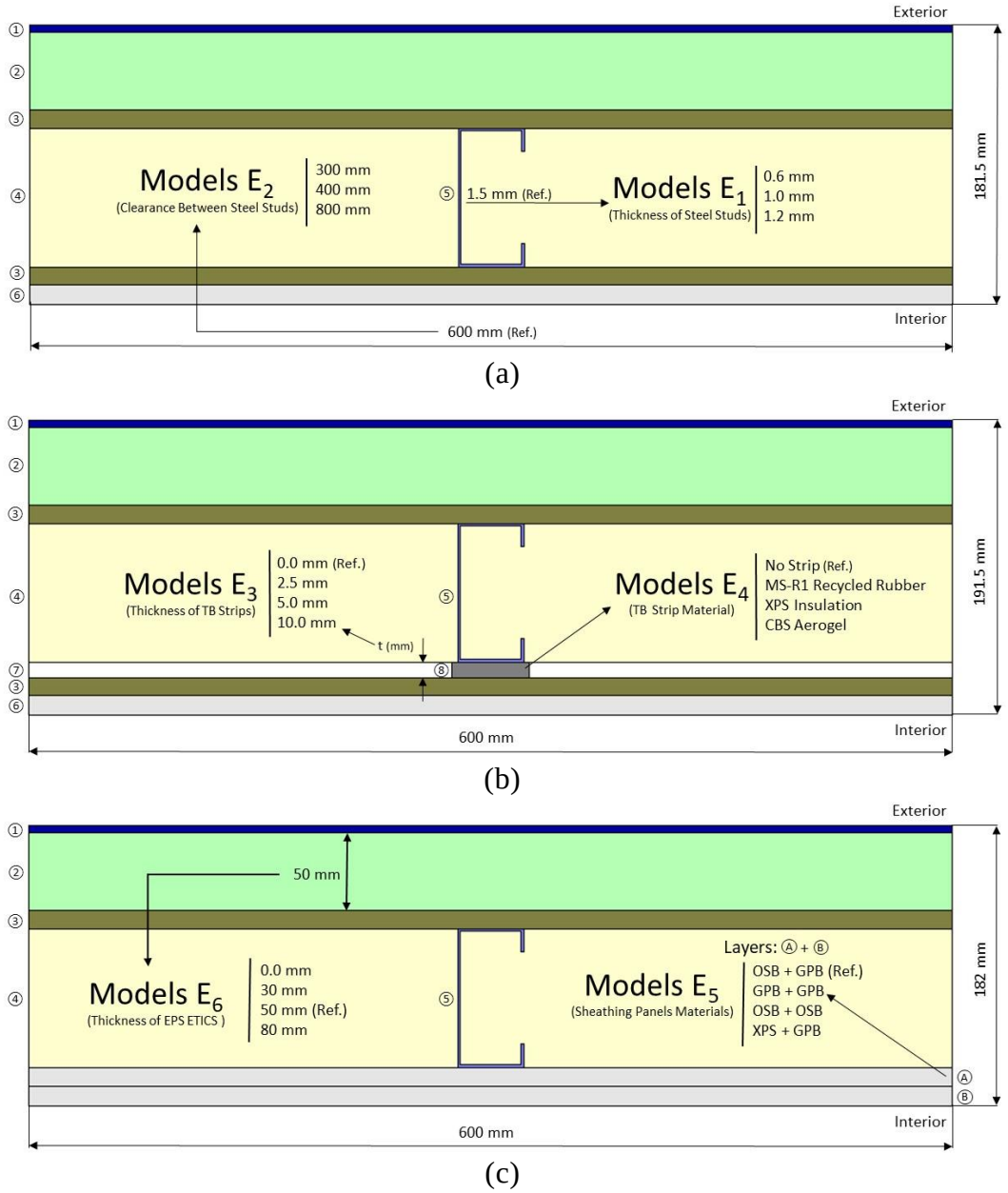

Figure 3.4 - Exterior LSF facade wall models cross-sections: (a) E1 and E2; (b) E3 and E4; (c) E5 and E6. Layers: ① ETICS finish; ② EPS; ③ OSB; ④ Mineral wool; ⑤ Steel stud C90; ⑥ Gypsum plasterboard (GPB); ⑦ Air layer; ⑧ TB strip (P. Santos et al., 2019).

3.2 Two-Dimension Numerical Simulation

The two-dimension numerical simulation was performed using the FEM software THERM (THERM, 2017). THERM uses two-dimensional (2D) conduction and radiation heat-transfer analysis based on the finite-element method, which can model building elements. This method requires that the cross section be divided into a mesh made up of non-overlapping elements.

In this section will be explained the conditions and parameters used for the numerical simulation using software THERM and some previous verifications to prove the software accuracy and to demonstrate skills to the correct use of this tool.

3.2.1 Verifications of 2D FEM Models

Previously to the usage of the THERM, the accuracy of the software should be verified. Firstly, the verification according to the Annex C from ISO 10211 (ISO 10211, 2017) should be performed. This verification process was successfully performed and will be described in the following section 4.2.3.

Another way to check the reliability of the 2D FEM models is to compare results obtained from numerical simulation with the analytical solution provided by ISO 6946 (ISO 6946, 2017) for a simplified model of the same wall, composed only by homogeneous layers, *i.e*. without the LSF structure. The obtained U-values for the analytical and numerical approaches are displayed in Table 3.6.

Table 3.6 – Thermal transmittance obtained for simplified wall models with homogeneous layers (P. Santos et al., 2019).

Wall typology (without steel frame)	***U*-value** [W/(m.K)]	
	Analytical	**2D FEM**[1]
Interior Reference Partition Wall	0.321	0.321
Exterior Reference Facade Wall	0.227	0.227

[1] using THERM software (THERM, 2017).

These results ensure the high accuracy for THERM software as well as the ability and skills to perform a correct usage of the tool.

3.2.2 Boundary Conditions

Before performing a numerical simulation, it is necessary to define the boundary conditions to be applied on the LSF walls. Regarding temperatures, it will be set the interior temperature as 20°C and the exterior temperature as 0°C (winter season). For the interior partition walls, the temperature of 10°C was set as the unconditioned space temperature, which means the side with the lowest temperature. Regarding surface thermal resistances it were used the values set on ISO 6946 (ISO 6946, 2017) for horizontal heat flow, *i.e.* 0.13 (m^2.K)/W and 0.04 (m^2.K)/W for internal (R_{si}) and external resistance (R_{se}), respectively. Emphasizing that, for the interior partition walls it was used internal surface resistances in both sides of the partition, *i.e.* 0.13 (m^2.K)/W.

3.2.3 Air layers Modelling

The air layers inside the walls were modelled as a solid-equivalent with the same thermal conductivity. The thermal resistance for these unventilated air-gaps were obtained in the ISO 6946 (ISO 6946, 2017). Knowing the thickness of the air-gap and dividing by its tabulated thermal resistance it was obtained the solid-equivalent thermal conductivity used in the 2D FEM numerical simulations, as displayed in Table 3.7.

Table 3.7 – Thermal resistances and equivalent thermal conductivities for air layers (P. Santos et al., 2019).

$\boldsymbol{d_{air}}$ [1] [mm]	$\boldsymbol{R_{air}}$ [2] [m^2.K/W]	$\boldsymbol{\lambda_{eq}}$ [3] [W/(m.K)]
2.5	0.055	0.045
5.0	0.11	0.045
10.0	0.15	0.067
90.0	0.18	0.500

[1] d_{air} – Thickness of air layer; [2] R_{air} – Thermal resistance of air layer (from ISO 6946); [3] λ_{eq} –Equivalent thermal conductivity.

3.2.4 Domain Discretization

The finite element mesh of a model in THERM software is controlled by two parameters: (*i*) quadtree mesh parameter and (*ii*) error estimator. The quadtree mesh parameter determines how

fine the mesh is, *i.e.* the maximum size of the initial element subdivision. The error estimator returns the percentage error energy norm, which is related to the gradient of heat flux (energy). If the returned value is greater than the target value, THERM refines the mesh in the areas with a high rate of change in the heat flux (Lawrence Berkeley Nation Laboratory, 2017).

For these simulations, the quadtree mesh was set to its standard value of 6, and the error estimator (maximum percentage of the error energy norm) was set at 2%. Once it was defined the cross-section's geometry, the material properties and the boundary conditions, the software THERM meshes the cross-section, performs the heat-transfer analysis, runs an error estimation (refines the mesh if necessary) and returns the converged solution.

3.3 Results and Discussions

After modelling and simulating all created wall models on software THERM, the results for LSF interior partition and exterior facade will be presented and remarked on the following sections.

3.3.1 LSF Interior Partition Walls

In Table 3.8 are displayed the obtained transmittance values for every wall model and all variations on the same parameter (values 1, 2 and 3). It is also represented the U-value for the interior reference wall, the absolute and percentage difference from each model to the reference value.

Table 3.8 – Thermal transmittance (U-value) obtained for LSF interior walls (P. Santos et al., 2019).

Wall Model	Evaluated Parameter	Ref. Value	Value 1	Value 2	Value 3
I1	**Thickness of Steel Studs** [mm]	**0.6**	**1.0**	**1.2**	**1.5**
	***U*-value** [W/(m^2.K)]	0.449	0.474	0.482	0.491
	Absolute difference	---	+0.025	+0.033	+0.042
	Percentage difference	---	+5.6%	+7.3%	+9.4%
I2	**Clearance Between Steel Studs** [mm]	**600**	**300**	**400**	**800**
	***U*-value** [W/(m^2.K)]	0.449	0.580	0.515	0.420
	Absolute difference	---	+0.131	+0.066	-0.029
	Percentage difference	---	+29.2%	+14.7%	-6.5%
I3	**Thickness of Aerogel TB[1] Strips** [mm]	**0.0**	**2.5**	**5.0**	**10.0**
	***U*-value** [W/(m^2.K)]	0.449	0.415	0.392	0.374
	Absolute difference	---	-0.034	-0.057	-0.075
	Percentage difference	---	-7.6%	-12.7%	-16.7%
I4	**TB[1] Strips Materials** [10 mm]	**---**	**MS-R1[2]**	**XPS[3]**	**CBS[4]**
	***U*-value** [W/(m^2. K)]	0.449	0.421	0.396	0.374
	Absolute difference	---	-0.028	-0.053	-0.075
	Percentage difference	---	-6.2%	-11.8%	-16.7%
I5	**Sheathing Panels**				
	GPB[5] Thickness [mm]	2×12.5	12.5	---	12.5
	OSB[6] Thickness [mm]	---	12.0	2×12.0	---
	XPS[3] Thickness [mm]	---	---	---	12.0
	***U*-value** [W/(m^2.K)]	0.449	0.419	0.397	0.338
	Absolute difference	---	-0.030	-0.052	-0.111
	Percentage difference	---	-6.7%	-11.6%	-24.7%

[1]TB – Thermal Break; [2]MS-R1 – Acousticork (rubber); [3]XPS – Extruded Polystyrene; [4]CBS – Cold Break Strip (Aerogel); [5]GPB – Gypsum Plaster Board; [6]OSB – Oriented Strand Board.

The same results are also graphically illustrated on Figure 3.5, where a bar graph characterize the percentage increase or decrease for each wall model in comparison with the reference wall value which is represented on the black bar.

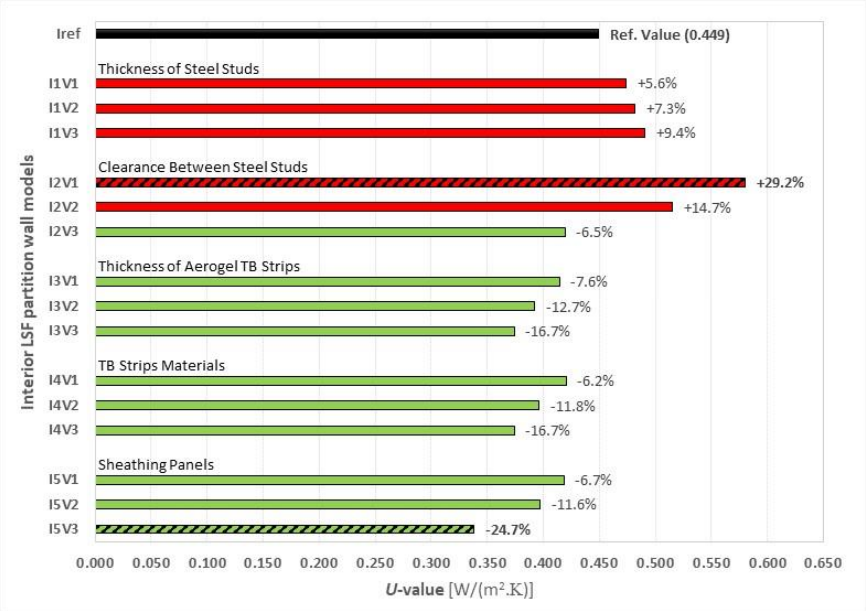

Figure 3.5 - Thermal transmittance (U-value) obtained for LSF interior walls (P. Santos et al., 2019).

It is possible to conclude that the LSF steel structure increases the thermal transmittance value of the wall in about 40% (+0.128 W/(m^2·K)), as the calculated U-value from the interior reference wall without steel frame is 0.321 W/(m^2·K) (Table 3.6) and the obtained value for the reference interior partition wall is 0.449 W/(m^2·K) (Table 3.8). This large increase in the U-value is a result of the high thermal conductivity of the steel (50.000 W/(m.K)) even for a very low thickness steel structure (0.6 mm) and also to the fact that the thermal insulations is not continuous, *i.e.* the internal mineral wool is bridged by the steel studs.

The first parameter assessed was the thickness of steel studs (models I1). As expected, as the amount of steel increases with higher thicknesses, also the U-value of the wall increases. When the thickness of the reference wall raised from 0.6 mm to 1.0 mm, 1.2 mm and 1.5 mm, the U-value had an increase of +5.6%, 7+.3% and +9.4%, respectively.

The parameter of the distance between the vertical studs (models I2) has the reference value of 600 mm. The decreasing of this distance to 300 mm and 400 mm brought an increasing on the wall's U-value of +29.2% and +14.7%, it was expected given the amount of steel per unit area has enlarged. On the other hand, the growing of distance from 600 mm to 800 mm resulted in a decrease of -6.5% on the wall's U-value.

Analysing the performance of the thermal break (TB) strip – models I3 – it is possible to conclude that the usage of a TB strip increase the insulation of the steel structure and consequently decreased the thermal transmittance of the wall, as expected (Table 3.8). The U-value reduction was of -7.6%, -12.7% and -16.7% for the aerogel TB strip with thicknesses of 2.5 mm, 5.0 mm, and 10.0 mm, respectively.

The influence of the TB strip material (10.0 mm) was evaluated on models I4. Using recycled rubber (MS-R1) as a thermal break material, the U-value reduction was about -6.2% when comparing with the reference wall model, without TB strip (Table 3.8). For the XPS TB strip, the U-value decreased -11.8% and using a TB strip made of aerogel the wall thermal transmittance has dropped even more (-16.7%). The strip made of aerogel provided the best results, but still being a quite expensive material in comparison with the other two (recycled rubber and XPS).

The wall models I5 presented the variation on the sheathing panels configurations according to what was presented on Table 3.2. The three variations for sheathing panels proposed resulted on better values than the interior reference wall, mostly because gypsum plasterboard has the highest thermal conductivity value, providing the uppermost U-value for the reference interior LSF partition wall (Table 3.8). The U-value reduction varies from -6.7% (GPB and OSB panels) up to -24.7% (GPB and XPS panels). This largest reduction was expected given the very reduced thermal conductivity of XPS material (0.037 W/(m.K)) in comparison with GPB (0.175 W/(m.K)) and OSB (0.100 W/(m.K)).

Regarding the major and minor obtained values, the highest thermal transmittance increased (+29.2%) was achieved on the model I2V1 and it corresponds to the shortest distance between steel studs (300 mm). The biggest thermal transmittance decreased (-24.7%) was reached on the model I5V3 and corresponds to a configuration with GPB and XPS sheathing panels. To better visualise and compare both wall models that had given the extreme U-values, the Figure 3.6 graphically display the temperature and heat flux for those models.

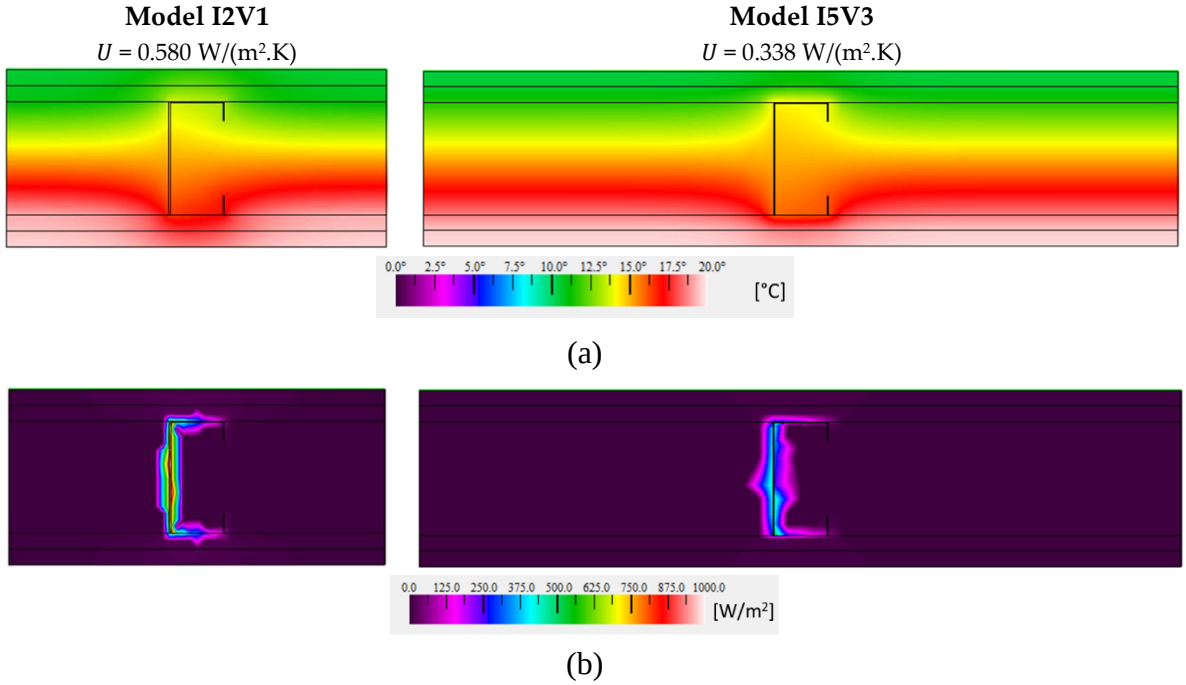

Figure 3.6 – Temperature (a) and heat flux (b) colour distribution for internal LSF wall models I2V1 and I5V3 (P. Santos et al., 2019).

The temperature distribution in both LSF wall cross-sections is very similar (Figure 3.6a), being well visible the influence of the steel stud in the temperature distribution, given the high thermal conductivity from steel and consequently thermal bridge effect. Analysing the heat flux images (Figure 3.6b) it is clear the high concentration of the heat flux around the steel stud. Moreover, there are higher heat flux values for model I2V1, *i.e.* the wall with 300 mm clearance between studs, in comparison to the other model.

These extreme U-values allow to verify the great steel relevance inside the LSF wall (models I2), as well as the big importance of providing a continuous thermal insulation layer (model I5V3), even with a small thickness (only 12.0 mm in each side). Additionally, this XPS sheathing layer has also the advantage of being an affordable solution when compared with more expensive material, e.g. the aerogel TB strips (models I3).

3.3.2 LSF Exterior Facade Walls

The thermal transmittance values obtained for the LSF exterior walls as well as the differences between each parameter and the exterior reference wall U-values are displayed on Table 3.9.

Table 3.9 – Obtained U-values for LSF exterior facade walls (P. Santos et al., 2019).

Model	Evaluated Parameter	Ref. Value	Value 1	Value 2	Value 3
E1	**Thickness of Steel Studs** [mm]	**1.5**	**0.6**	**1.0**	**1.2**
	***U*-value** [W/(m^2.K)]	0.276	0.267	0.272	0.274
	Absolute difference	---	-0.009	-0.004	-0.002
	Percentage difference	---	-3.3%	-1.4%	-0.7%
E2	**Clearance Between Steel Studs** [mm]	**600**	**300**	**400**	**800**
	***U*-value** [W/(m^2.K)]	0.276	0.323	0.299	0.263
	Absolute difference	---	+0.047	+0.023	-0.013
	Percentage difference	---	+17.0%	+8.3%	-4.7%
E3	**Thickness of Aerogel TB[1] Strips** [mm]	**0.0**	**2.5**	**5.0**	**10.0**
	***U*-value** [W/(m^2.K)]	0.276	0.263	0.255	0.248
	Absolute difference	---	-0.013	-0.021	-0.028
	Percentage difference	---	-4.7%	-7.6%	-10.1%
E4	**TB[1] Strips Materials** [10 mm]	---	**MS-R1[2]**	**XPS[3]**	**CBS[4]**
	***U*-value** [W/(m^2.K)]	0.276	0.265	0.256	0.248
	Absolute difference	---	-0.011	-0.020	-0.028
	Percentage difference	---	-4.0%	-7.2%	-10.1%
E5	**Inner Sheathing Panels**				
	GPB[5] Thickness [mm]	12.5	2×12.5	---	12.5
	OSB[6] Thickness [mm]	12.0		2×12.0	---
	XPS[3] Thickness [mm]	---	---	---	12.0
	***U*-value** [W/(m^2.K)]	0.276	0.282	0.271	0.256
	Absolute difference	---	+0.006	-0.005	-0.020
	Percentage difference	---	+2.2%	-1.8%	-7.2%
E6	**Thickness of EPS[7] ETICS[8]** [mm]	**50**	**0**	**30**	**80**
	***U*-value** [W/(m^2.K)]	0.276	0.494	0.327	0.223
	Absolute difference	---	+0.218	+0.051	-0.053
	Percentage difference	---	+79.0%	+18.5%	-19.2%

[1]TB – Thermal Break; [2]MS-R1 – Acousticork (rubber); [3]XPS – Extruded Polystyrene; [4]CBS – Cold Break Strip (Aerogel); [5]GPB – Gypsum Plaster Board; [6]OSB – Oriented Strand Board; [7]EPS – Expanded Polystyrene: [8]ETICS – External Thermal Insulation Composite System.

For a better visualization and easier analyse the same results are also graphically illustrated on Figure 3.7 for all modelled parameters showing the obtained U-values and its percentage differences.

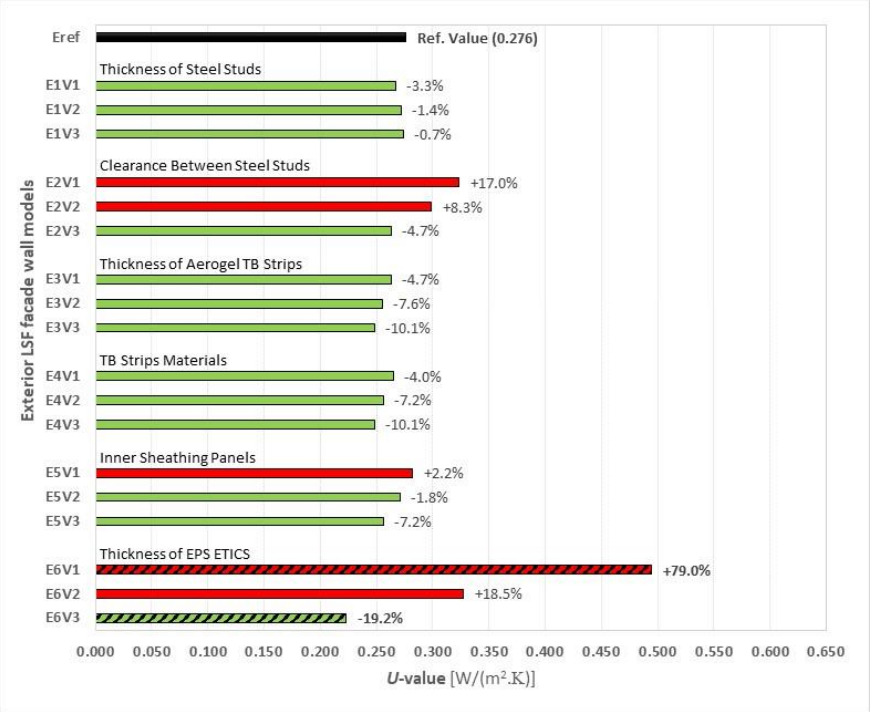

Figure 3.7 – Obtained U-values for LSF exterior facade walls (P. Santos et al., 2019).

To evaluate the influence of the steel structure on the exterior wall U-value it was compared the result obtained for the wall without steel frame – from Table 3.6, 0.227 W/(m^2.K) – with the U-value computed for the reference exterior wall – from Table 3.9, 0.276 W/(m^2.K). The thermal transmittance increase due to the steel frame was of 0.049 W/(m^2.K), which represents 22% higher. This increment in the U-value is much lower when compared with the interior partition wall: +0.128 W/(m^2.K) or +40%. This reduced relevance of the steel structure in the exterior partition wall, even having a steel thickness more than a double from the interior wall (1.5 mm instead of 0.6 mm), could be justified by the continuous thermal insulation used in the ETICS (hybrid LSF structure), while in the interior partition wall all the thermal insulation is inside the wall and bridged by the steel studs (cold LSF structure).

For the steel structure thickness on exterior walls (models E1) when the thickness is reduced from 1.5 mm to 0.6 mm a small decrease of -3.3% on the wall U-value occurs. In the other hand, in the interior partition wall, the corresponding value when the thickness enhanced from 0.6 mm to 1.5 mm, was from an increase of +9.4% on the U-value (Table 3.9), confirming the higher relevance of the amount of steel in the interior partition wall.

The second evaluated parameter is the distance between the vertical studs (models E2), where the reference value is 600 mm. When decreasing the distance between the studs – 300 mm and

400 mm – the wall U-value increases by +17.0% and +8.3%, respectively. Instead, when the clearance between vertical studs were bigger (800 mm) the U-value decreases -4.7%. These variations on the thermal transmittance are closely related with the amount of steel inside each wall configuration.

The outcomes of the thickness variation for the aerogel thermal break strip were computed using the models E3 (Table 3.9). As expected, with the addition and increasing on the TB thickness (2.5 mm, 5.0 mm and 10.0 mm) resulted on a decrease of the wall U-value by -4.7%, -7.6% and -10.1%, respectively. Confronting these results with the similar ones for interior partition wall (-7.6%, -12.7% and -16.7% from Table 3.8), it can be highlighted that the decrease on U-values is now considerably lower. This could be justified by the reduced importance of the steel frame in the exterior walls and that, therefore the effect of the TB strips is also reduced.
The wall models E4 evaluated the effectiveness of different materials for the 10 mm thick TB strip and, as expected, the aerogel strip permitted the biggest reduction on wall thermal transmittance (-10.1%), followed by XPS strip (-7.2%) and the recycled rubber (-4.0%).

Regarding the innermost sheathing panels parameters evaluated on models E5, three different configurations were assessed (Table 3.9). The first configuration was composed by two panels of GPB and obtaining an increase of +2.2% on the U-value when comparing with the reference value. The second configuration used two panels of OSB and presented a U-value reduction of -1.8%. For the last variation, the internal layers were composed by a GPB and XPS panels, resulting on the most significant reduction: -7.2%. Comparing the result of this parameter with the values computed for the same parameter on the interior partition wall (-24.7%), the U-value reduction for exterior wall are significantly lower. It is also explained by the existence of the ETICS continuous thermal insulation in the exterior facade wall, which decreases the steel frame thermal bridges transmission. Therefore, the relevance of an extra continuous thermal insulation layer becomes also reduced.

The influence of the EPS thickness in the ETICS are evaluated on the models E6, being the reference value for exterior wall (50 mm of EPS) compared with the three additional values: 0 mm, 30 mm and 80 mm. Evidently this was the most relevant evaluated parameter, leading to an increase in the U-value of +79% (model E6V1) when there is no exterior thermal insulation and a reduction of -19.2% when the EPS thickness was increased to 80 mm (model E6V3).

The models which obtained the highest and the lowest U-values have the colour temperature and heat flux displayed on Figure 3.8. Analysing the temperature distribution on Figure 3.8a it is very clear the influence of the continuous thermal insulation on model E6V3 (hybrid LSF

structure) providing higher temperature around the steel frame in comparison with model E6V1 (cold frame LSF structure). Looking at the heat flux distribution (Figure 3.8b), again it its visible the influence of the thermal insulation layer, as the model E6V3 presents lower heat transfer rate around the steel frame than in the model E6V1.

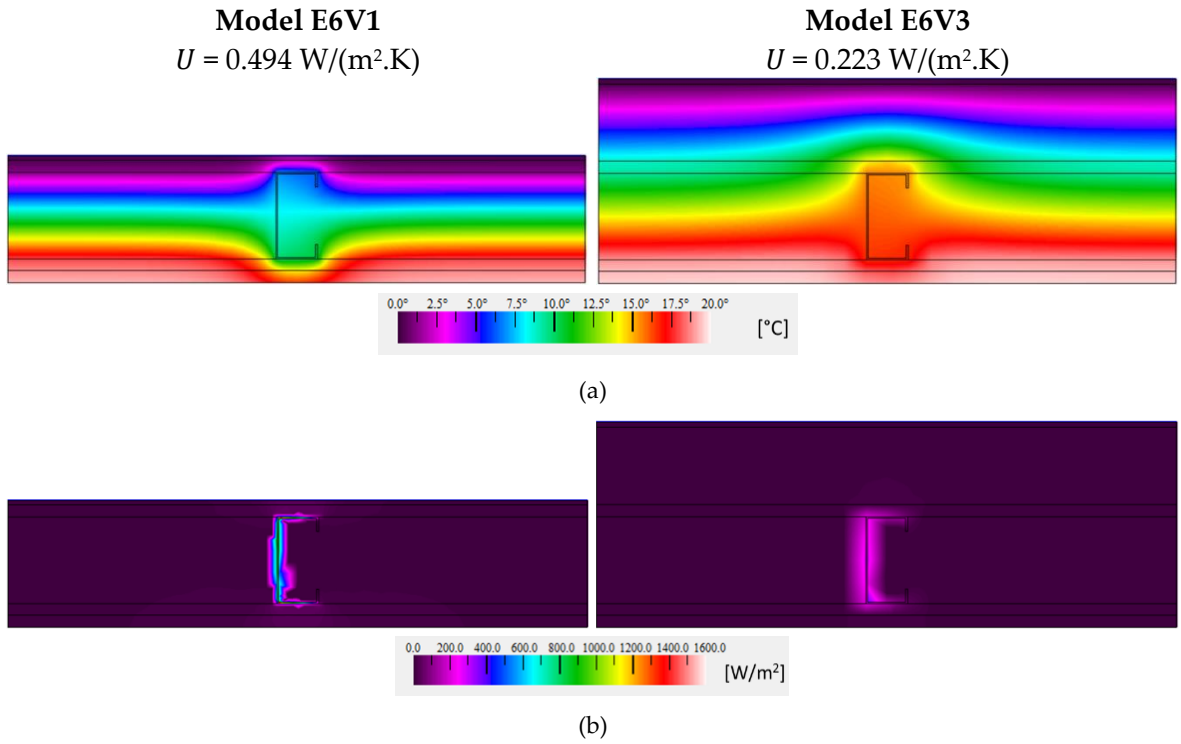

Figure 3.8 – Temperature (a) and heat flux (b) colour distribution for LSF exterior wall models with the highest U-value increase and decrease (E6V1 and E6V3) (P. Santos et al., 2019).

3.3.3 Overall Comparison

The interior partition LSF wall presented a higher U-values and a greater influence of the internal steel structure on the wall thermal transmittance. This was expected given the high thermal conductivity of steel and the absence of a continuous thermal insulation on interior partition walls which highlight the thermal bridges effects of the LSF structure and results on higher U-values. However, a higher heat flux through the interior walls allows that other evaluated parameters have a greater influence on wall thermal transmittance. The distance between steel studs brought increases in the U-value up to +29.2%, while the XPS sheathing panel results in a decrease of up to -24.7% in the U-value.

For partition walls with no external continuous insulation, the more the metal structure get thicker more the thermal transmittance increases, up to +9.4% (for 1.5 mm). The usage of thermal break strips allowed to reduce the U-value up to -16.7% (10 mm aerogel strip). As the thermal transmittance depends on the thermal conductivity of the materials, the U-value reduction for the other material 10mm TB strips was of: -6.2% for recycled rubber, -11.8% for XPS and -16.7% for aerogel.

For the exterior facade LSF walls, the existence of an ETICS continuous thermal insulation on the outer side reduces the heat flux through the wall, specially through the steel frame, resulting on a lower wall U-value and decreasing the importance of other evaluated parameters. The U-value highest increment and decrement was found in the parameter thickness of EPS insulation on ETICS layer where an increase of +79.0% when there was no EPS (0.0 mm) and a decrease of -19.2% for an EPS with 80mm.

Other ways to demonstrate how the continuous insulation reduces the influence of the other evaluated parameters on the exterior facade walls is to compare the performance of some parameters on both walls. On exterior walls, when the thickness of the steel structure gets thinner (from 1.5 mm to 0.6 mm) the U-value reduces only in -3.3% (-0.009 W/(m^2.K)). However, when in the interior partition wall, the steel structure becomes thicker in the same proportion (from 0.6 mm to 1.5 mm), the absolute U-value increase in more than four times (+0.042 W/(m^2.K)).

Again, on exterior facade walls, the decreasing of the distance between the steel studs by half – from 600 mm to 300 mm – doubling the amount of steel in the same area, increased the U-value by only +17.0% (+0.047 W/(m^2.K)). Meanwhile, on interior partition walls, for the same change in parameter, the absolute U-value increased was of almost the triple, +0.131 W/(m^2.K).

The use of aerogel TB strips with different thicknesses in exterior facade walls allowed a reduction of the U-value up to -10.1% (-0.028 W/(m^2.K)). For the interior partition wall, the same parameter brought an absolute U-value reduction of more than a double (-0.075 W/(m^2.K)). For the 10 mm TB strip with different material (rubber, XPS and aerogel) allowed a decrease in the exterior wall U-value to about -4.0% (-0.011 W/(m^2.K)), -7.2% (-0.020 W/(m^2.K)) and -10.1% (-0.028 W/(m^2.K)), respectively. In the interior wall these U-value reductions were quite higher: -6.2% (-0.028 W/(m^2.K)), -11.8% (-0.053 W/(m^2.K)) and -16.7% (-0.075 W/(m^2.K)), respectively.

The use of different inner sheathing panels (GPB, OSB and XPS) allowed to obtain a U-value variation down to -7.2% (-0.020 W/(m^2.K)) for the XPS/GPB panels in exterior facade walls.

In the interior partition wall, the absolute U-value reduction was much more relevant, resulting on a value more than five times higher (-0.111 W/(m^2.K)). This was due not only to the absence of any continuous thermal insulation in the reference interior LSF wall, but also to the fact that in this case the two wall sides were updated with a XPS sheathing panel (one in each side), while in the exterior facade only the inner wall surface was updated with a XPS sheathing panel.

4 ACCURACY COMPARISSON BETWEEN ANALYTICAL METHODS TO COMPUTE *U*-VALUE

In the literature there are several analytical methods to compute the thermal resistance and transmittance of LSF buildings elements. However, any research work comparing the accuracy of these analytical methodologies was found in the bibliography.

The work presented in this chapter was subject of the paper "Analytical Methods to Estimate the Thermal Transmittance of LSF walls: Calculation Procedure Review and Accuracy Comparison" (P. Santos et al., 2020) which the main objective is to compare the accuracy performance of the six analytical methodologies known from the literature.

4.1 LSF Wall Models Description

In this work, all the evaluated walls were derived from a typical reference exterior LSF wall (hybrid frame construction), as illustrated and described before on Section 3.1.2 from the previous chapter.

Some parameters and variables on the reference LSF wall (Figure 3.3), were modified to obtain the 80 different LSF walls models that were used in this work. The modified parameters, listed on Table 4.1, were: (*i*) the cold formed steel studs, (*ii*) the cavity batt insulation, (*iii*) the exterior continuous insulation and (*iv*) the studs facing sheathing materials.

Table 4.1 – Modified parameters and variables to reach 80 wall models, and range of the U-values obtained on the simulations (P. Santos et al., 2020).

Parameter	**Variable**		**Evaluated Values**	***U*-value** [W/(m^2.K)] (Min – Max.)
Steel Studs	Spacing [mm]		300, 400, **600***, 800	0.260 – 0.319
	Depth [mm]		**90***, 150, 170, 200 (Pertecno, 2015)	0.199 – 0.272
	Thickness [mm]		0.6, 1.0, 1.2, **1.5***, 2.0	0.264 – 0.274
	Flange [mm]		**43***, 70 (Pertecno, 2015)	0.272 – 0.223
Cavity Insulation	Thickness [mm]	**C90***	0, 45, **90***	0.272 – 0.489
		C150	0, 75, 150	0.224 – 0.489
		C170	0, 85, 170	0.223 – 0.489
		C200	0, 100, 200	0.199 – 0.489
	Thermal Conductivity [W/(m.K)]	AIB[1]	0.018 (Thermablok, 2011)	0.153 – 0.287
		MW*[2]	**0.035*** (Volcalis, 2019)	0.199 – 0.381
Exterior Insulation (ETICS[10])	Thickness [mm]		0, 5, 10, 15, 20, 30, **50***, 80	0.221 – 0.869
	Thermal Conductivity [W/(m.K)]	**EPS***[3]	**0.036*** (TincoTerm, 2015)	0.221 – 0.869
		ICB[4]	0.045 (C. Santos & Matias, 2006)	0.246 – 0.346
Sheathing	Thermal Conductivity [W/(m.K)]	**OSB***[5]	**0.100*** (KronoSpan, 2019)	0.221 – 0.983
		GPB*[6]	**0.175*** (Gyptec Ibérica, 2019)	
		CWB[7]	0.220 (Viroc, 2019)	
		FCB[8]	0.390 (Equitone, 2012)	
		GRB[9]	0.500 (GRCA, 2018)	

*Reference value; [1]AIB - Aerogel Insulation Blanket; [2]MW - Mineral Wool; [3]EPS - Expanded Polystyrene; [4]ICB - Insulation Cork Board; [5]OSB - Oriented Strand Board; [6]GPB - Gypsum Plaster Board; [7]CWB - Cement Wood Board; [8]FCB - Fiber Cement Board; [9]GRB - Glass-fiber Reinforced Board; [10]ETICS - Exterior Thermal Insulation Composite System.

Regarding the steel studs, were used studs type C with web depth varying from 90 mm to 200 mm, resulting on four steel stud's sizes: C90, C150, C170 and C200. For the space between the vertical studs, were modelled walls with four different values (300 mm to 800 mm range). Relating to the steel stud thickness, five values were used, ranging from 0.6 mm to 2.0 mm. Two different studs flange lengths were used on the wall models: 43 mm and 70 mm, obtained from a cold formed steel profiles manufacturer catalogue (Pertecno, 2015).

Concerning the thickness of the cavity insulation material, three different levels were evaluated: empty cavity (no insulation); half of the cavity filled, and full-filled cavity. Also, two different insulation materials were considered: mineral wool (MW) and aerogel insulation blanket (AIB), a higher performance insulation material.

For the exterior continuous insulation (ETICS), eight different thicknesses from the insulation main material were evaluated, ranging from 0 to 80 mm. Moreover, two different insulation materials were considered: the reference one, expanded polystyrene (EPS), and the insulation cork board (ICB).

Finally, for the sheathing layers parameter, three other different materials were used, besides the reference OSB and GPB panels, they are: cement wood board (CWB), fiber cement board (FCB) and glass-fiber reinforced board (GRB).

LSF walls are usually classified as warm, hybrid and cold frame construction depending on the its thermal insulation type and location, *i.e.*, whether it is a cavity batt insulation and/or exterior continuous thermal insulation (P. Santos et al., 2012). Table 4.2 displays the total number of LSF walls evaluated (80 models) as well as the number of LSF walls by frame type: (*i*) warm, (*ii*) hybrid or (*iii*) cold.

Table 4.2 – Number of evaluated LSF walls by frame type and range of obtained thermal transmittances (U-values) (P. Santos et al., 2020).

Frame type	**Number of Evaluated LSF Walls**	***U*-value** [W/(m^2.K)]	
		Min.	**Max.**
Warm	22	0.348	0.983
Hybrid	43	0.153	0.608
Cold	15	0.384	0.869
Total	80	0.153	0.983

Additionally, it is also shown in Table 4.2, the range of U-values from the wall models evaluated, being the minimum thermal transmittance equal to 0.153 W/(m^2.K) for a hybrid frame construction, while the maximum value is 0.983 W/(m^2.K) for warm frame construction.

4.2 Numerical FEM Method

In this work the numerical computational tool used was the two-dimensional (2D) Finite Element Method (FEM) THERM software (Lawrence Berkeley Nation Laboratory, 2017). For all wall models the maximum error admitted on THERM was 2%.

To verify the accuracy of the numerical methods available, the standard ISO 10211 (ISO 10211, 2017) provides, in Annex C, the specifications to evaluate the precision of the numerical algorithm used by following and performing two test reference cases (Case 1 and 2) and comparing the given results. In order to be classified as a two-dimension steady-state high precision method, the calculation software algorithm should give the requested results on both test reference cases.

In the next sub-sections will be presented the boundary conditions and air layer modelling used on the THERM simulations, as well as the two test reference cases verification and an experimental laboratory validation.

4.2.1 Boundary Conditions

After modelling the walls on the software, the boundary conditions must be defined before running the model. The temperatures from inside and outside environments were set to 20°C (interior) and 0°C (exterior), respectively. The surface thermal resistances values used in the simulations were obtained from ISO 6946 (ISO 6946, 2017) for horizontal heat flow: 0.13 (m^2.K)/W for internal thermal resistance (R_{si}) and 0.04 (m^2.K)/W for external thermal resistance (R_{se}). Additionally, two adiabatic surfaces were defined on both extremities LSF wall model cross-sections.

4.2.2 Air Layers Modelling

Some wall models evaluated do not present a full-filled insulation cavity or have an empty air cavity, being necessary to model air gaps inside the LSF wall. The thermal resistance of those unventilated air layers were modelled as a solid-equivalent using the thermal conductivity (λ) calculated from the thermal resistances values prescribed on ISO 6946 (ISO 6946, 2017) for horizontal heat flow.

4.2.3 ISO 10211 Test Cases Verification

To ensure the accuracy of the FEM THERM software (THERM, 2017) in modelling heat transfer models it was performed the two test reference cases (Case 1 and 2) proposed on the standard ISO 10211 (ISO 10211, 2017). In both test cases, the difference between the standard solution for each reference point and the temperature computed by the algorithm should not exceed 0.1°C.

Test case 1 provided a sketch of a half square column with 28 grid points placed equidistantly, which the corresponding temperatures for each point are known. The Figure 4.1a shows the temperature distribution for the given initial and boundary conditions. The calculated temperatures values for each 28 reference grid points are displayed on Figure 4.1b, being all the same as provided by ISO 10211.

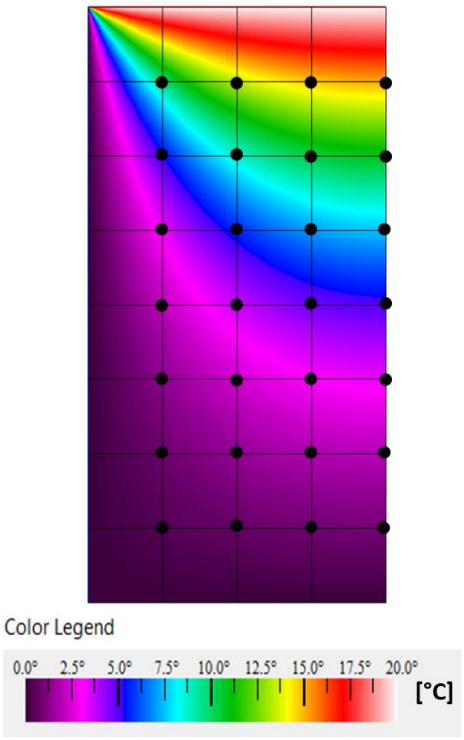

(a)

Temperatures [°C]			
9.7	13.4	14.7	15.1
5.2	8.6	10.3	10.8
3.2	5.6	7.0	7.5
2.0	3.6	4.7	5.0
1.3	2.3	3.0	3.2
0.7	1.4	1.8	1.9
0.3	0.6	0.8	0.9

(b)

Figure 4.1 - Obtained results for test case 1: (a) temperature distribution, (b) computed temperatures for each point at the column.(P. Santos et al., 2020)

In the test case 2, a different model was proposed to be evaluated by the numerical model. Beside the temperature distribution, the heat flow calculated is also validated and shall not exceed 0.1 W/m from the reference value. The Figure 4.2a illustrates the computed temperature distribution and the points where the reference temperature is provided (points A to I). THERM results for temperatures and heat flow are displayed on the chart of Figure 4.2b.

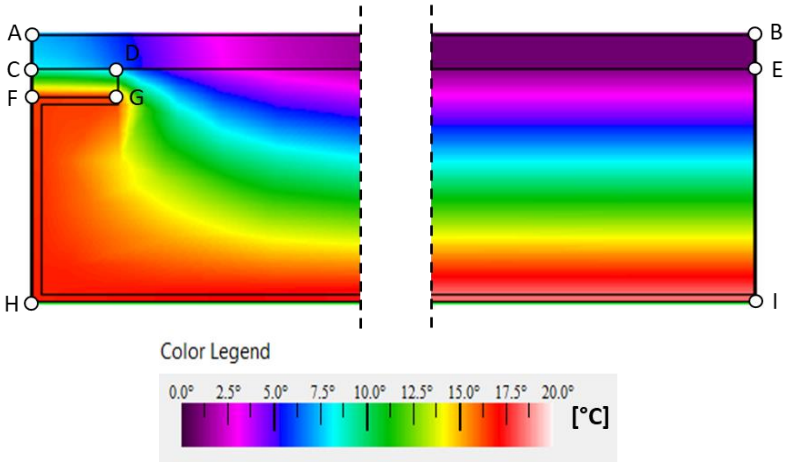

(a)

Points	Temperatures [°C]
A	7.1
B	0.8
C	7.9
D	6.3
E	0.8
F	16.4
G	16.3
H	16.8
I	18.3
Heat flow rate 9.49 W/m	

(b)

Figure 4.2 – ISO 10211 test case 2 obtained results: (a) temperature distribution, (b) computed values for each point (P. Santos et al., 2020).

For all proposed points, temperatures computed were exactly the same prescribed by ISO 10211 and heat flow rate was only 0.01 W/m below the reference value (9.5 W/m), but still under the difference limit of 0.1 W/m.

Those results prove not only that the software THERM fulfil the requirements from ISO 10211 to be considered a two-dimensional steady-state high precision method, but also that it is being used correctly.

4.2.4 Experimental Validation

To validate the numerical simulation results provided by THERM software, used as reference values to evaluate the accuracy of the analytical calculations, some LSF walls were thermally evaluated on a laboratory facility. In these experiments it was used the heat flow meter (HFM) method as prescribed in standard ISO 9869-1 (ISO 9869-1, 2014).

For these laboratory evaluations were used an equipment formed by two small thermal insulated boxes: a hot and a cold one. Those insulated boxes ensure a controlled temperature gradient between both surfaces of a sample wall, which is placed between then as shown on Figure 4.3.

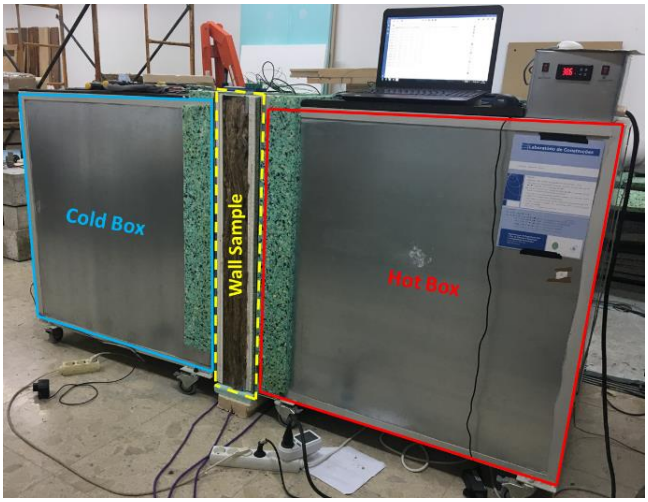

Figure 4.3 – Hot e cold boxes apparatus evaluating a specimen wall.

The hot box is powered by a 70 watts electrical resistance and has an internal system which control the inside temperature to be around 40ºC (Figure 4.4a). Its internal system is set to turns the resistance on until the internal temperature reach 42ºC, then turns it off, turning it on again when the temperature drops to 38 ºC.

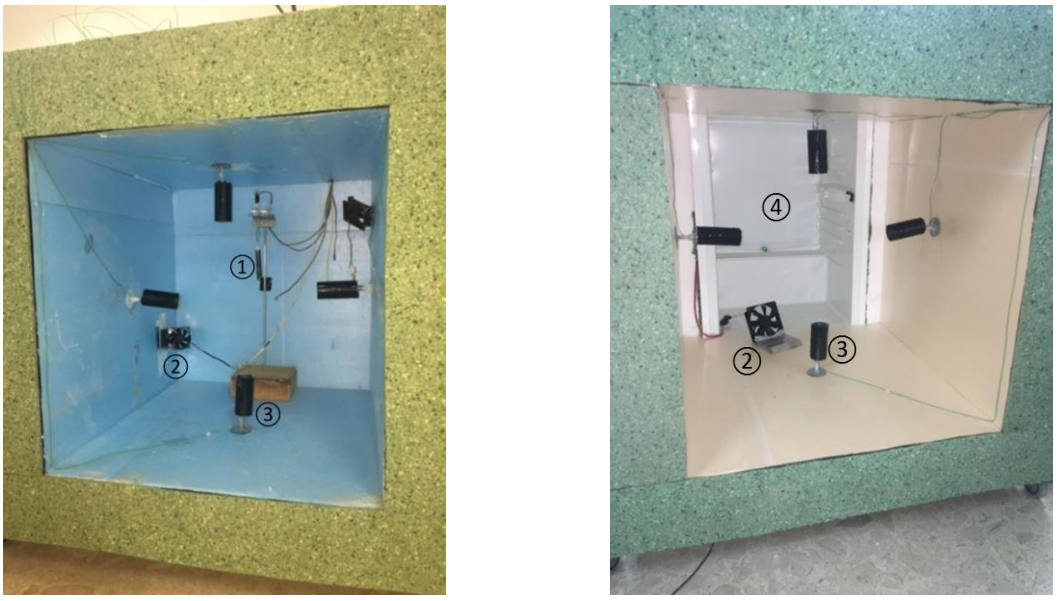

(a) (b)

Figure 4.4 – Internal details from boxes: (a) hot box; (b) cold box. ① Electric Resistance, ② Fan, ③ Thermocouples, ④ Refrigerator.

The cold box (Figure 4.4b) is cooled by a refrigerator that is attached to the back of the box. The refrigerator is controlled by its own thermostat and is set to the lowest temperature managing to maintain an average temperature of 5ºC. Each box is internally insulated with XPS boards to ensure a stable inner environment and minimize heat loss. Small fans are used to uniformize the air temperature inside each box, mitigating the risk of air temperature stratification.

The small-scale wall specimen used in this laboratory equipment have dimensions of 1030 x 1060 mm. For theses experimental validation, the small-scale LSF walls have cold formed steel profiles C90 (90×43×15×1.5 mm) spaced 400 mm. The design of the LSF frame is detailed on Figure 4.5.

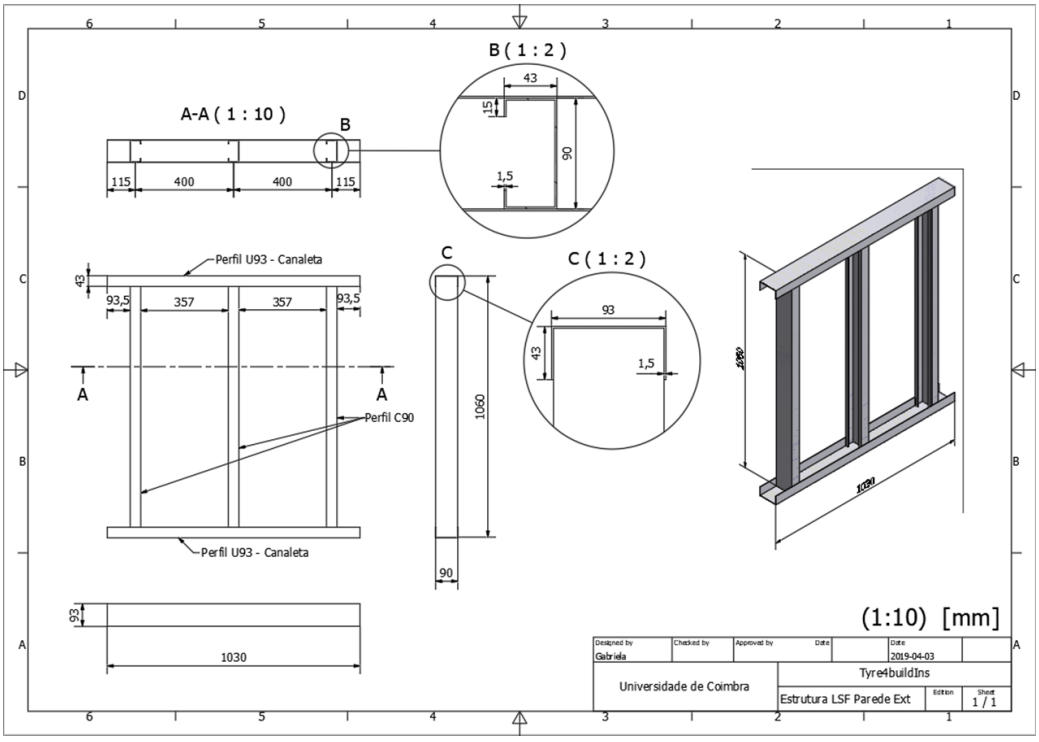

Figure 4.5 – Detailed design of the LSF steel structure.

During the experiment, the heat flow was measured by Hukseflux HFP01 (precision ±3%) heat flux meters (Hukseflux, 2016), placed in two different locations on the wall surface in each side: (*i*) over the location of the vertical stud (HFM1) and (*ii*) in the middle distance between the vertical profiles (HFM2), over the insulation cavity (Figure 4.6).

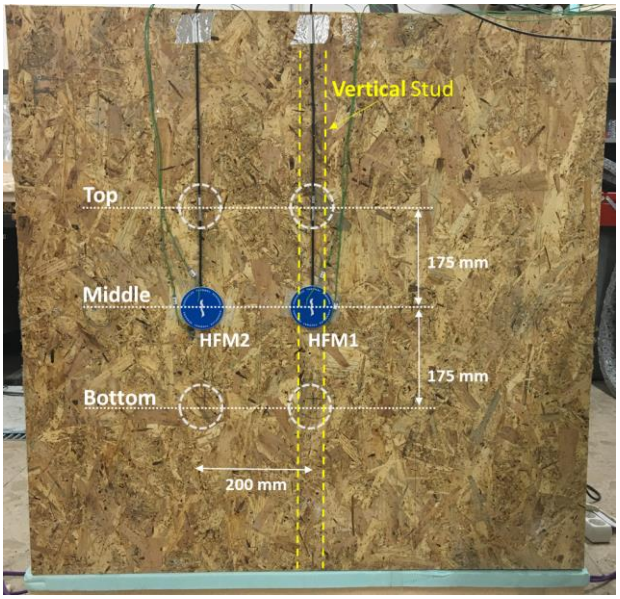

Figure 4.6 - Sensors locations on exterior wall surface (HFM – Heat Flux Meter; TC - Thermocouples) of the specimen wall.

The temperature measurements were performed by 12 thermocouples type K (chromel-alumel), placed six in each box (hot and cold), computing both the surface and environment air temperatures. The data collected during the experiment tests (temperatures and heat fluxes) were recorded by two Pico TC-08 data-loggers (precision ±0.5ºC) and analysed through the PicoLog 6 software (Figure 4.7).

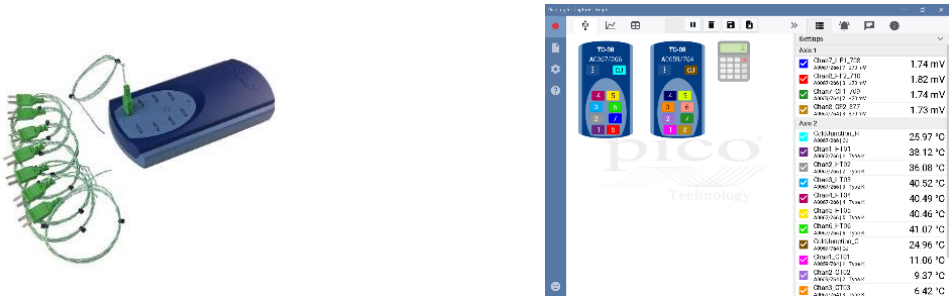

(a) (b)

Figure 4.7 – PicoLog data acquisition system: (a) TC-08 data-logger; (b) PicoLog 6 software screen (Pico Technology, 2019).

Previous to the experimental tests, a calibration procedure was performed on the 12 thermocouples and the data acquisition system to adjust the errors of each sensor. The calibrations equations and procedures are explained on Appendix A.

The LSF wall experimental tests lasts 24 hours being performed three tests for every wall, one for each height location of the heat flow meters: (*i*) top, (*ii*) middle and (*iii*) bottom positions (Figure 4.6), where the value considered for U-value calculation on each position was the average of the three tests.

The heat flow meter method, prescribed in standard ISO 9869-1 (ISO 9869-1, 2014) was used to calculate the U-value, which return two slightly different U-values: (*i*) a higher value for the stud location position and (*ii*) a lower value for the clear wall position. The overall U-value of the wall was obtained by computing an area weighted of both U-values. The steel stud influence zone area was defined as prescribed on the ASHRAE zone method, explained on Section 2.6.3.1.

For this experimental validation, two different LSF walls were tested to validate the numerical simulations: (*i*) an air cavity wall and (*ii*) a mineral wool (MW) insulation filled cavity wall. The exterior and interior sheathing materials were the same for both walls: an OSB layer (12 mm) attached to each side of the C90 steel stud and a gypsum plasterboard (12.5 mm) as the innermost layer. The overall U-values measured during the experimental tests and the U-values estimated by 2D FEM numerical simulations (THERM) are displayed on Table 4.3.

Table 4.3 – U-values measured in laboratory tests and calculated by THERM (P. Santos et al., 2020).

Wall Type	**Test**	**Sensors location**	***U*-value** [W/(m^2 .K)]
Air cavity LSF Wall	1	Top	1.984
	2	Middle	2.001
	3	Bottom	1.922
		Average Measured	**1.969**
		Estimated by THERM	**1.931**
		Percentage Error	-2%
MW LSF Wall	1	Top	0.602
	2	Middle	0.614
	3	Bottom	0.648
		Average Measured	**0.621**
		Estimated by THERM	**0.621**
		Percentage Error	0%

According to the results from laboratory tests, the U-value calculated by the numerical simulation THERM matches exactly the measure value, 621 W/(m^2.K), on the wall with the mineral wool on the cavity (MW LSF). For the air cavity LSF wall, the estimate value (1.931 W/(m^2.K)) was slightly lower than the measured one (1.969 W/(m^2.K)) resulting on an error of 2%. Despite the uncertainties present on laboratory tests, such as equipment and sensors precision, and also the FEM numerical simulation predicted error (under 2%), these results can reiterate the reliability of the software THERM to predict the thermal transmission values on this type of LSF walls and ensure the quality of the thermal transmittance values used as reference values in this work.

4.3 Analytical Methods Calculation

As previously detailed, the methods for analytical approach for thermal resistance and transmittance of a construction element will be used to evaluate 80 different LSF wall models being compared with the value calculated by numerical FEM method.

In order to perform the comparison between the numerical results and every analytical method previously analysed, it was developed an Excel spreadsheet (Figure B.1) to consolidate and automate the calculation processes. This spreadsheet was programmed in a way that the data and the details of the cross-section of each wall models must be entered just once, and the program will perform the whole calculation of R-values and U-values for the six different methods, using the Equations previously presented. In Appendix C are displayed the description of all 80 wall models, the evaluated parameters and the numerical simulation result on Table C.1. On Table C.2 is displayed the results for the six analytical calculation methods.

For the ASHRAE Modified Zone method calculation processes, the chart provided in Figure 2.5 were replaced by the adjusted curves chart for C90 and C150 obtained from the reference (ASHRAE, 2017) and illustrated in Figure 4.8. For the stud's sizes C170 and C200 it was not possible to adjust curves as the original graphic do not contemplate these stud sizes. Thus, it was assumed by approximation, that the zf factor for stud size C170 were like the ones provided by the C150 curve. Regarding the LSF walls with C200 steel studs, they were not computed by this method in this work (five LSF wall models).

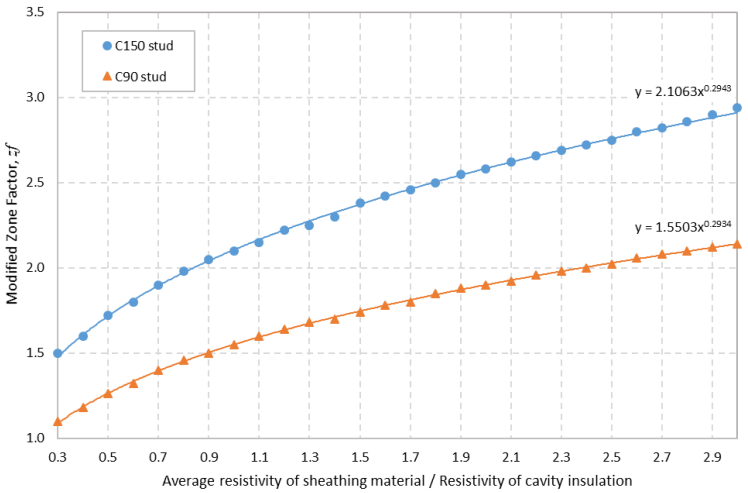

Figure 4.8 - Modified zone factor curves for LSF walls (P. Santos et al., 2020).

4.4 Results and Discussions

The thermal transmittance values obtained by the six analytical methods for all evaluated walls are plotted on Figure 4.9. Each point in these graphics represents a different LSF wall model, being the value on the horizontal axis the reference U-value provided by the numerical 2D FEM simulations and used as reference values, while the value on the vertical axis is the analytical U-value computed by the respective method: (a) ISO 6946 Combined Method; (b) Gorgolewski Method 1; (c) Gorgolewski Method 2; (d) Gorgolewski Method 3; (e) ASHRAE Zone Method, and; (f) Modified Zone Method.

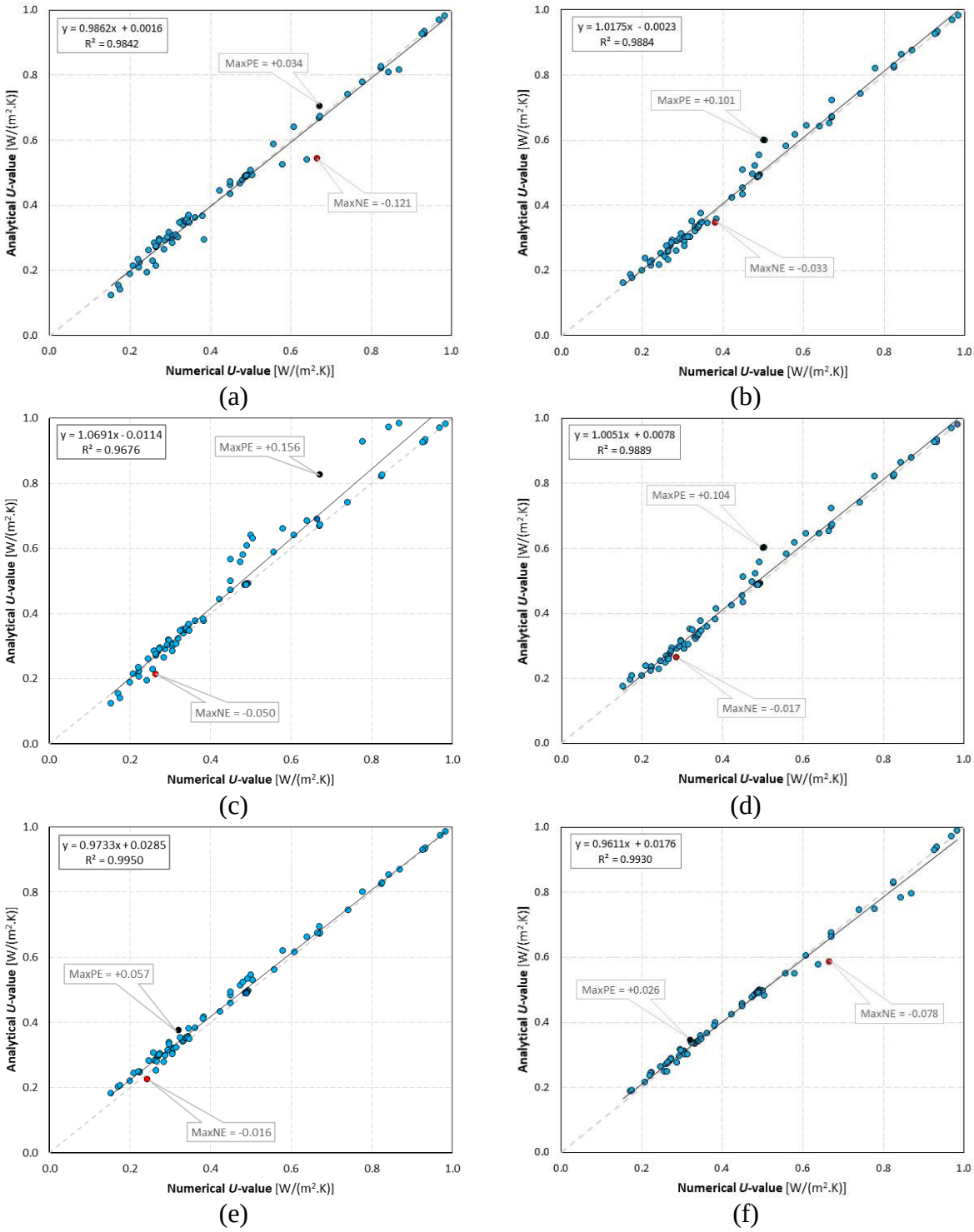

Figure 4.9 - Thermal transmittances (*U*-values) comparison between the evaluated analytical methods and the numerical 2D FEM results used as reference: (a) ISO 6946 Combined Method; (b) Gorgolewski Method 1; (c) Gorgolewski Method 2; (d) Gorgolewski Method 3; (e) ASHRAE Zone Method, and; (f) Modified Zone Method (P. Santos et al., 2020).

Also represented in each method graphics are: (*i*) a linear trend-line, (*ii*) the R-squared coefficient of determination, (*iii*) the maximum positive error (MaxPE), (*iv*) the maximum negative error (MaxNE) and (*v*) a 45 degrees inclination line, that corresponds to ideal match between the analytical and the numerical method.

Standing out that the linear trend-lines and the corresponding correlation factors are not the most adequate features to quantify the precision of each analytical method, since they do not correlate the analytical U-values (y axis) with the numerical ones (x axis) instead, they correlate the analytical values with its corresponding trend-line, which could be very different from the 45° line (ideal match line).

In general, it is possible to conclude that there is a quite good agreement between the U-values provided by the analytical methods evaluated and the numerical reference ones, evidencing a good accuracy of these analytical methods.

The Gorgolewski Method 2 shows off the largest dispersion of values (Figure 4.9c) – mainly for U-values greater than 0.4 W/(m^2.K) – and the smallest correlation coefficient (0.9676). Also, its linear trend line has the biggest slope (1.069) being above from the ideal inclination line (45°). Moreover, the major positive error (MaxPE) was found in this analytical method (+0.156 W/(m^2.K)), which correspond to a cold framed (without ETICS) wall model with the air cavity 50% filled with mineral wool.

The major negative error (MaxNE) – a value of -0.121 W/(m^2.K) – was found in the ISO 6946 Combined Method (Figure 4.9a). This LSF wall model is cold framed (without ETICS) using GRB sheathing panels. Surprisingly, the Combined Method should not be applicable to building elements where insulation is bridged by metal (what happens in cold and hybrid LSF walls), even so the results presented have a very good accuracy.

Both ASHRAE Methods presents very good correlation factor: 0.995 and 0.993. ASHRAE Zone Method (Figure 4.9e) features a good accuracy for thermal transmittance values higher than 0.6 W/(m^2.K) while, for lower values, presents a more conservative trend – U-values bigger than the reference ones. In contrast, Modified Zone Method (Figure 4.9f) has a good precision on lower U-values (smaller than 0.6 W/(m^2.K)) but presenting an overoptimistic trend, *i.e.* U-values smaller than the reference ones.

It was also computed the root mean square error (RMSE) in absolute value and in percentage as shown on Figure 4.10. Each bar chart contains the maximum positive error (MaxPE) and the maximum negative error (MaxNE).

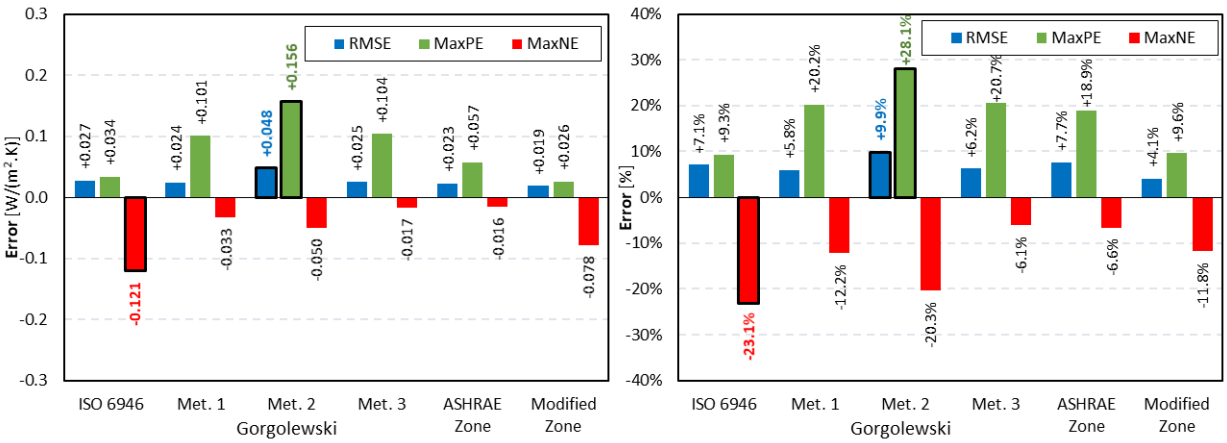

(a) (b)

Figure 4.10 – *U*-values error for all wall models: (a) Absolute errors; (b) Percentage errors (P. Santos et al., 2020).

When analysing the calculated errors for each analytical method it is possible to say that Gorgolewski Method 2 show off the biggest RMSE (+0.048 W/(m^2.K); +9.9%) and also the higher maximum positive error (+0.156 W/(m^2.K); +28.1%), confirming a not very good accuracy of this method. The smaller RMSE was found on the Modified Zone Method: +0.019 W/(m^2.K); +4.1%. This analytical method also has the lowest percentage MaxPE (+9.6%), confirming the relatively good accuracy of this method.

Looking through the RMSE percentage values, the analytical methods can be classified, according their accuracy performance, from best to worst, as follows: (1) ASHRAE Modified Zone Method (+4.1%), (2) Gorgolewski Method 1 (+5.8%); (3) Gorgolewski Method 3 (+6.2%); (4) ISO 6946 Combined Method (+7.1%); (5) ASHRAE Zone Method (+7.7%), and (6) Gorgolewski Method 2 (+9.9%).

In order to provide a different perception of the accuracy of the analytical methods, the 80 wall models were separated by frame type (warm, hybrid and cold) to perform a similar analysis. The results were compiled in the chart on Figure 4.11 that displays the percentage RMSE for all wall models, now grouped by frame type.

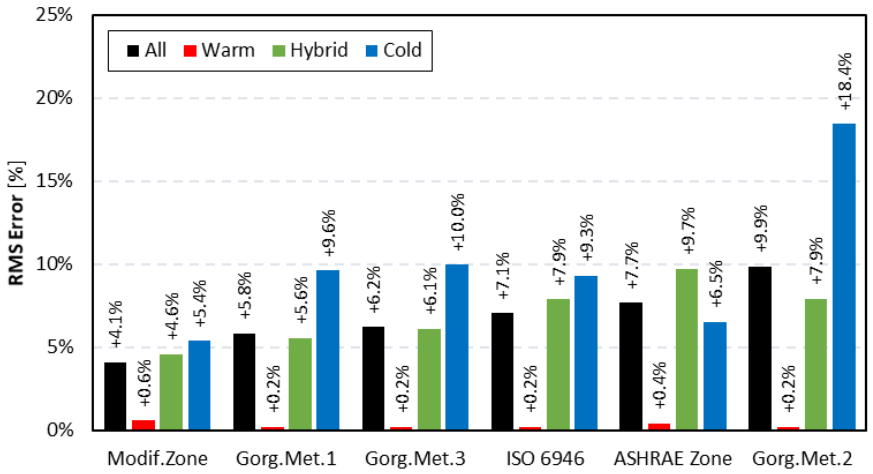

Figure 4.11 – Percentage RMSE from evaluated analytical methods (P. Santos et al., 2020).

For all LSF walls evaluated (black bar on Figure 4.11), the *U*-value errors vary from 4.1% (ASHRAE Modified Zone) to 9.9% (Gorgolewki Method 2).

The highest percentage RMSE normally happen in the cold frame walls, followed by hybrid and warm frame walls, with an only exception, on ASHRAE Zone Method, where the hybrid frame showed of the higher error (9.7%) instead of the cold frame (6.5%). This different behaviour can be related with the non-continuous thermal insulation that increases the errors in the analytical approach for cold frame walls, however, providing minor errors when there is only external insulation (warm frame walls).

The highest RMS *U*-value error occurred in cold frame walls calculated by the Gorgolewski Method 2 (18.4%), while for the same frame type the smaller error occurs in the Modified Zone Method (5.4%).

Regarding the hybrid frame wall models, the highest error occurred on the ASHRAE Zone method (9.7%) while the lowest happened in the Modified Zone Method (4.6%), confirming the good accuracy of this method.

5 CONCLUSIONS

The parametric study carried out on two different types of LSF walls focused on the measurement of the thermal bridges' effects and the evaluation of some strategies to mitigate them. These mitigation strategies can decrease the effects of the thermal bridges caused by the steel structure on LSF walls, increasing these walls' thermal performance and reducing the energy consumption of the buildings where LSF construction system has been used.

The comparison and evaluation of some analytical methods to calculate the thermal transmittance for LSF walls complemented the study on the thermal evaluation of the LSF walls, since it allowed to conclude that these methods have relatively good precisions. Which means that they have undergone successfully adaptations on their unidimensional models to consider the effects of the lateral heat flow originated by steel studs. Also served to reiterate the importance of the continuous thermal insulation to mitigate the harmful effects of thermal bridges on the thermal transmittance of LSF walls.

5.1 General Conclusions

In Chapter 3, a sensitivity analysis regarding the thermal transmittance (U-value) was performed for two different types of lightweight steel framed (LSF) walls: interior partition and exterior facade. The numerical results were obtained by using 2D finite element method (FEM) – software THERM – that was previously verified according to the ISO 10211 and compared with an analytical approach by ISO 6946.

Some parameters were assessed for both wall's type, such as: (*i*) thickness of steel studs, (*ii*) distance between studs, (*iii*) thermal break strip thickness, (*iv*) thermal break strip material, (*v*) configuration of internal sheathing panels and, (*vi*) thickness of EPS on ETICS (only for external facade walls). The results of this parametric study were compared to the reference LSF walls: interior partition (0.449 W/(m^2.K)) and exterior façade (0.276 W/(m^2.K)).

The interior partition wall, as expected, showed high U-values and a greater influence of the internal steel structure on the wall thermal transmittance, given mostly by the absence of a

continuous thermal insulation which potentiate the effects of the thermal bridges. Higher heat flux through the interior walls result on a great influence of other parameters evaluated on the thermal transmittance of the wall. On the other hand, for the exterior facade wall, the existence of a continuous thermal insulation (ETICS) on the outer side reduces the heat flux through the wall, resulting on a lower U-value and in a lower effect of the thermal bridges.

In Chapter 4, the accuracy of six analytical methods to compute the thermal transmittance of LSF walls was evaluated. These methodologies were described and applied to estimate the U-values of 80 LSF walls, being their precision evaluated by comparison with the results provided by 2D FEM numerical simulations, which were experimentally validated.

For each method evaluated, the trend-lines and respective correlation coefficients were obtained. It was also computed the Root Mean Square Error (RMSE), the Maximum Positive Error (MaxPE) in absolute and percentage values, as well as the Maximum Negative Error (MaxNE) for each method for all LSF walls. The results were displayed for each method and also for each frame type: (*i*) warm; (*ii*) hybrid, and; (*iii*) cold.

It was possible to conclude that the evaluated analytical methods disclosed a quite good accuracy performance, as the RMSE values fluctuated from 0.019 W/(m^2.K) to 0.048 W/(m^2.K), in percentage, between 4.1% and 9.9%. The maximum positive and negative U-values errors were +0.156 W/(m^2.K) and -0.121 W/(m^2.K), respectively (+28.1% and -23.1%). According to the thermal insulation configuration (warm, hybrid or cold frames) of the LSF walls, the precision of the analytical methods variates. On the warm frames walls the precision of the analytical calculation was the highest, as the biggest RMSE (0.6% in Modified Zone Method) was a very low value. Following by the hybrid frames walls, where the highest error was 9.7% (Zone Method) and then, the cold frame walls with RMSE up to 18.4% (Gorgolewski Method 2).

When analysing the obtained U-values RMSE of all evaluated LSF walls (80 models), the best accuracy was demonstrated by Modified Zone Method (4.1%). The least accurate results were verified on Gorgolewski Method 2 (9.9%), which also provide the higher maximum positive error (+0.156 W/(m^2.K); +28.1%), evidencing some trend to provide conservative U-values. In sequence of accuracy, the other two Gorgolewski methods (1 and 3) were ranked as second (5.8%) and third place (6.2%) respectively.

The Combined Method, as described on ISO 6946 standard, exclude from the scope of its method the construction elements where the insulation is bridged by metal (cold and hybrid frames). Surprisingly, the Combined Method results were quite good, and it was ranked as

fourth best accurate methodology exhibiting better performance (7.1%) than other two analytical methods, which were specifically developed for LSF elements. However, the use of this analytical method should be performed with some cautions since it was the one that provided the larger negative error (-0.121 W/(m^2.K); -23.1%), evidencing some trend to provide over-optimistic U-values.

5.2 Future Work

In order to become a more complete approach on the thermal performance of LSF walls, the following steps of this work can be proceeding with the 3D numerical modelling and become able to investigate more deeply the transverse effects of the thermal bridges on thermal transmission of LSF walls. This way, it is possible to better understand the harmful effects of thermal bridges increasing the chance to be more assertive when using strategies to mitigate them. Also, with a better understanding to three-dimensional effects of the heat flow through the steel structure, make it possible to coming up with new adjustments to one-dimensional analytical methodologies for U-value calculation.

REFERENCES

Abu-Jdayil, B., Mourad, A. H., Hittini, W., Hassan, M., & Hameedi, S. (2019). Traditional, state-of-the-art and renewable thermal building insulation materials: An overview. *Construction and Building Materials*, *214*, 709–735. https://doi.org/10.1016/j.conbuildmat.2019.04.102

Asdrubali, F., Alessandro, F. D., Schiavoni, S., D'Alessandro, F., & Schiavoni, S. (2015). A review of unconventional sustainable building insulation materials. *Sustainable Materials and Technologies*, *4*, 1–17. https://doi.org/10.1016/j.susmat.2015.05.002

ASHRAE. (2017). *Handbook of Fundamentals (SI Edition)*.

Aslani, A., Bakhtiar, A., & Akbarzadeh, M. H. (2019). Energy-efficiency technologies in the building envelope: Life cycle and adaptation assessment. *Journal of Building Engineering*, *21*(March 2018), 55–63. https://doi.org/10.1016/j.jobe.2018.09.014

Balaji, N. C., Mani, M., & Venkatarama, R. (2013). Thermal performance of the building walls. *Building Simulation Applications - IBPSA Italy Conference, February 2013*.

Bellahcene, L., Cheknane, A., Bekkouche, S. M. A., & Sahel, D. (2017). The effect of the thermal inertia on the thermal transfer in building wall. *E3S Web of Conferences*, *22*. https://doi.org/10.1051/e3sconf/20172200013

Doran, S. M., & Gorgolewski, M. T. (2002). *BRE Digest 465 - U-values for light steel-frame construction*.

Equitone. (2012). *Fiber Cement Board*.

European Union. (2018). Directive (EU) 2018/844 of the European Parliament and of the Council of 30 May 2018 amending Directive 2010/31/EU on the energy performance of buildings and Directive 2012/27/EU on energy efficiency. In *Official Journal of the European Union* (Vol. 2018, Issue May, pp. 75–91).

Gorgolewski, M. (2007). Developing a simplified method of calculating U-values in light steel framing. *Building and Environment*, *42*(1), 230–236.

GRCA. (2018). *Practical Design Guide for Reinforced Concrete (GRC)* (March 2018).

Gyptec Ibérica. (2019). *Technical sheet: Standard gypsum plasterboard (in Portuguese)*. https://www.gyptec.eu/documentos/Ficha_Tecnica_Gyptec_A.pdf

Harvey, L. D. D. (2009). Reducing energy use in the buildings sector: Measures, costs, and examples. *Energy Efficiency*, *2*(2), 139–163. https://doi.org/10.1007/s12053-009-9041-2

Henriques, J., Rosa, N., Gervasio, H., Santos, P., & Simões, L. (2017). Structural performance of light steel framing panels using screw connections subjected to lateral loading. *Thin Walled Structures*, *121*(January), 67–88. https://doi.org/10.1016/j.tws.2017.09.024

Hukseflux. (2016). *Hukseflux Thermal Sensors User Manual HFP01* (pp. 1–43). https://www.hukseflux.com/sites/default/files/product_manual/HFP01_HFP03_manual_v1721.pdf

IEA - International Energy Agency. (2016). *World Energy Outlook 2016, Paris: OECD/IEA*. www.iea.org/t&c

IEA - International Energy Agency. (2018). *Key world energy statistics*. https://doi.org/10.1002/art.1780270204

ISO 10211. (2017). *Thermal bridges in building construction — Heat flows and surface temperatures — Detailed calculations*.

ISO 6946. (2017). *Building components and building elements — Thermal resistance and thermal transmittance — Calculation methods*.

ISO 8990. (1994). *Thermal insulation - Determination of steady-state thermal transmission properties - Calibrated and guarded hot box, International Organization for Standardization*.

ISO 9869-1. (2014). *Thermal insulation - Buildins elements - In-situ measurement of thermal resistance and thermal transmittance - Part 1: Heat flow meter method* (p. 36).

Kaynakli, O. (2012). A review of the economical and optimum thermal insulation thickness for building applications. *Renewable and Sustainable Energy Reviews*, *16*(1), 415–425. https://doi.org/10.1016/j.rser.2011.08.006

Kendrick, C., Ogden, R., Wang, X., & Baiche, B. (2012). Thermal mass in new build UK housing : A comparison of structural systems in a future weather scenario. *Energy & Buildings*, *48*, 40–49. https://doi.org/10.1016/j.enbuild.2012.01.009

Kosny, J., Christian, J. E., Barbour, E., & Goodrow, J. (1994). *Thermal Performance of Steel-Framed Walls*.

KronoSpan. (2019). *Technical sheet: KronoBuild OSB 3*. https://de.kronospan-express.com/public/files/downloads/kronobuild/kronobuild-en.pdf

Lawrence Berkeley Nation Laboratory. (2017). *THERM 7 NFRC Simulation Manual* (Issue July). https://windows.lbl.gov/sites/default/files/Downloads/NFRCSim7-July2017.pdf

Martins, C., Santos, P., & Da Silva, L. S. (2016). Lightweight steel-framed thermal bridges mitigation strategies: A parametric study. *Journal of Building Physics*, *39*(4), 342–372. https://doi.org/10.1177/1744259115572130

MS-R1. (2017). *Acousticork MS-R1 Recycled rubber*. https://amorimcorkcomposites.com/media/1334/acousticork-book-en.pdf

Oktay, H., Tutumlu, H., & Yumrutaş, R. (2017). Comparison of Experimental and Literature models for the Heat Gain through the Walls in terms of the Effect of Thermophysical Properties. *12th International Conference on Latest Trends in Engineering and Technology (ICLTET'2017)*. https://doi.org/10.15242/iie.e0517016

Pertecno. (2015). *Catálogo Light Steel Frame*. http://www.pertecno.pt/pdf/Catálogo - Light Steel Framing.pdf

Pico Technology. (2019). *PicoLog 6 Software*. Version 6.1.10; Pico Technology. https://www.picotech.com/downloads

Pulselli, R. M., Simoncini, E., & Marchettini, N. (2009). Energy and emergy based cost-benefit evaluation of building envelopes relative to geographical location and climate. *Building and Environment*, *44*(5), 920–928. https://doi.org/10.1016/j.buildenv.2008.06.009

Rowley, F. B., & Algren, A. B. (1937). Thermal conductivity of building materials. *Engineering Experiment Station. Bulletin Nº 12*, 144. https://conservancy.umn.edu/bitstream/handle/11299/124246/eng_ex_bulletin_12.pdf?sequence=1&isAllowed=y

Sadineni, S. B., Madala, S., & Boehm, R. F. (2011). Passive building energy savings: A review of building envelope components. *Renewable and Sustainable Energy Reviews*, *15*(8), 3617–3631. https://doi.org/10.1016/j.rser.2011.07.014

Santos, C., & Matias, L. (2006). *ITE50 - Coeficientes de Transmissão Térmica de Elementos da Envolvente dos Edifícios (in Portuguese)*. LNEC - Laboratório Nacional de Engenharia Civil.

Santos, P., Lemes, G., & Mateus, D. (2019). Thermal Transmittance of Internal Partition and External Facade LSF Walls : A Parametric Study. *Energies*, *12*(14). https://doi.org/10.3390

Santos, P., Lemes, G., & Mateus, D. (2020). Analytical Methods to Estimate the Thermal Transmittance of LSF Walls : Calculation Procedures Review and Accuracy Comparison. *Energies*, *13*(4). https://doi.org/10.3390/en13040840

Santos, P., Silva, L. S. da, & Ungureanu, V. (2012). *Energy Efficiency of Light-weight Steel-framed Buildings* (1st ed.). European Convention for Constructional Steelwork (ECCS), Technical Committee 14 - Sustainability & Eco-Efficiency of Steel Construction, ISBN 978-92-9147-105-8, N. 129.

Soares, N., Martins, C., Gonçalves, M., Santos, P., Simões da Silva, L., & Costa, J. J. (2019). Laboratory and in-situ non-destructive methods to evaluate the thermal transmittance and behaviour of walls, windows, and construction elements with innovative materials: a review. *Energy & Buildings*, *182*, 88–110.

Soares, N., Santos, P., Gervasio, H., & Costa, J. J. (2017). Energy efficiency and thermal performance of lightweight steel-framed (LSF) construction: A review. *Renewable and Sustainable Energy Reviews*.

Spacetherm. (2018). *Technical sheet: Cold bridge strip*. https://www.proctorgroup.com/assets/Datasheets/Spacetherm_CBS_Datasheet.pdf

Tadeu, A., Simões, I., Simões, N., & Prata, J. (2011). Simulation of dynamic linear thermal bridges using a boundary element method model in the frequency domain. *Energy & Buildings*, *43*(12), 3685–3695.

THERM. (2017). *Software version 7.6.1* (7.6.1). Lawrence Berkeley National Laboratory, United States Department of Energy. https://windows.lbl.gov/software/therm

Thermablok. (2011). *Thermablok® Aerogel Insulation Blanked*. www.thermablok.co.uk

TincoTerm. (2015). *Technical sheet: EPS 100 (in Portuguese)*. http://www.lnec.pt/fotos/editor2/tincoterm-eps-sistema-co-1.pdf

Vijayalakshmi, M., Natarajan, E., & Shanmugasundaram, V. (2006). Thermal Behaviour of Building Wall Elements. *Journal of Applied Sciences*, *6*, 3128–3133. https://doi.org/10.3923/jas.2006.3128.3133

Viroc. (2019). *Cement Wood Board*.

Volcalis. (2019). *Technical sheet: Alpha mineral wool (in Portuguese)*. https://www.volcalis.pt/categoria_file_docs/fichatecnica_volcalis_alpharolo-253.pdf

WeberTherm Uno. (2018). *Technical specifications: Weber Saint-Gobain ETICS finish mortar (in Portuguese)*. Saint-Gobain Weber Portugal, S.A. https://www.pt.weber/files/pt/2019-04/FichaTecnica_weberthermuno.pdf

APPENDICES

A THERMOCOUPLES CALIBRATION

The equipment set calibrated is composed by two data logger Pico TC-08 and 12 thermocouples type K (chromel-alumel). For the calibration procedure the thermocouples were already connected to the data logger, 6 thermocouples in each data logger, as shown on Figure A.1a.

(a) (b)

Figure A.1 – Calibration procedure: (a) thermocouples connected to data loggers; (b) thermostatic and agitated bath machine.

For this calibration, the thermocouples type K were placed inside the thermostatic bath machine (Figure A.1b), where the temperature and agitation of the water were controlled. For a period of 5 minutes, the sensors were submitted to each level of temperature, starting with a 5°C bath. The temperature of the bath was raised in 5°C on each level change, ending on 45°C.

The average measures from each thermocouple on every level of temperature were exported to an Excel spreadsheet and using the tendency line tool, plotting its calibration equation as illustrated on Figure A.2.

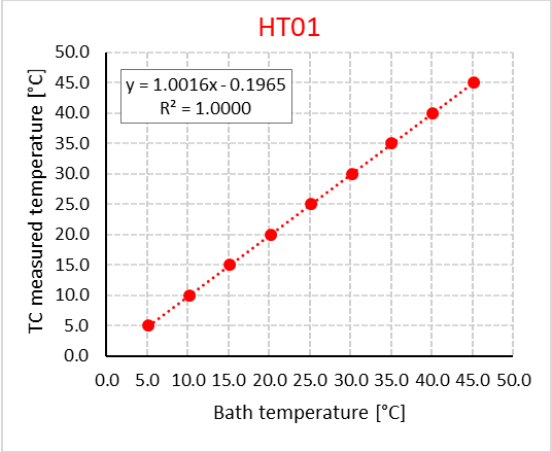

Figure A.2 - Thermocouple HT01 charter, its tendency line and calibrations equation.

The average temperature measured by the 12 thermocouples for every level of thermostatic bath are shown on Table A.1, which also indicates the average error for each thermocouple.

Table A.1 - Average measured temperature for each thermocouple on every level of thermostatic bath.

Bath temperature (°C)	5	10	15	20	25	30	35	40	45	Average Error
HT01	5.15	10.20	15.18	20.21	25.14	30.18	35.07	40.13	45.15	**0.156**
HT02	5.08	10.13	15.11	20.13	25.07	30.12	35.01	40.07	45.09	**0.090**
HT03	4.99	10.01	14.99	20.01	24.94	29.99	34.87	39.94	44.95	**-0.034**
HT04	4.77	9.76	14.73	19.75	24.66	29.73	34.60	39.66	44.67	**-0.296**
HT05	4.67	9.62	14.60	19.62	24.55	29.60	34.49	39.55	44.56	**-0.414**
HT06	4.90	9.87	14.85	19.87	24.81	29.85	34.75	39.80	44.81	**-0.165**
CT01	5.31	10.35	15.34	20.36	25.30	30.33	35.23	40.28	45.31	**0.312**
CT02	5.23	10.25	15.24	20.26	25.20	30.23	35.13	40.19	45.21	**0.216**
CT03	5.12	10.10	15.08	20.11	25.04	30.07	34.98	40.03	45.05	**0.064**
CT04	4.92	9.88	14.86	19.90	24.83	29.87	34.77	39.83	44.84	**-0.144**
CT05	4.84	9.78	14.75	19.80	24.75	29.78	34.67	39.72	44.73	**-0.240**
CT06	5.08	10.05	15.02	20.06	25.02	30.03	34.93	39.98	44.99	**0.017**

After using the calibrating equations for each thermocouple, the results are much closer for the real values of the controlled temperature baths and can be verified by the low average errors for every thermocouple as indicated the Table A.2.

Table A.2 – Average measure temperature for each thermocouple already adjusted by its calibration equation.

Bath temperature (°C)	**5**	**10**	**15**	**20**	**25**	**30**	**35**	**40**	**45**	**Average error**
HT01	4.96	10.02	15.00	20.04	24.99	30.03	34.93	39.99	45.03	**0.000**
HT02	4.97	10.02	15.01	20.04	24.98	30.03	34.93	40.00	45.02	**0.001**
HT03	4.98	10.02	15.00	20.04	24.97	30.04	34.93	40.00	45.03	**0.000**
HT04	5.00	10.00	15.00	20.03	24.96	30.04	34.93	40.01	45.03	**0.000**
HT05	5.03	9.99	14.98	20.02	24.97	30.03	34.94	40.01	45.03	**0.000**
HT06	5.01	10.00	14.99	20.03	24.98	30.03	34.94	40.00	45.03	**0.000**
CT01	4.96	10.02	15.02	20.04	24.98	30.03	34.93	39.99	45.03	**0.000**
CT02	4.98	10.01	15.01	20.04	24.98	30.02	34.94	40.00	45.03	**0.000**
CT03	5.01	10.00	14.99	20.03	24.97	30.02	34.94	40.00	45.03	**0.000**
CT04	5.02	9.99	14.98	20.03	24.97	30.03	34.94	40.01	45.03	**0.000**
CT05	5.03	9.98	14.97	20.03	24.99	30.03	34.93	40.00	45.03	**-0.001**
CT06	5.01	9.99	14.98	20.03	25.00	30.03	34.94	40.00	45.02	**0.000**

After the equipment set calibration procedure is finished, thermocouples must no longer be disconnected from the data loggers, otherwise it should be calibrated again.

B CALCULATION SPREADSHEET

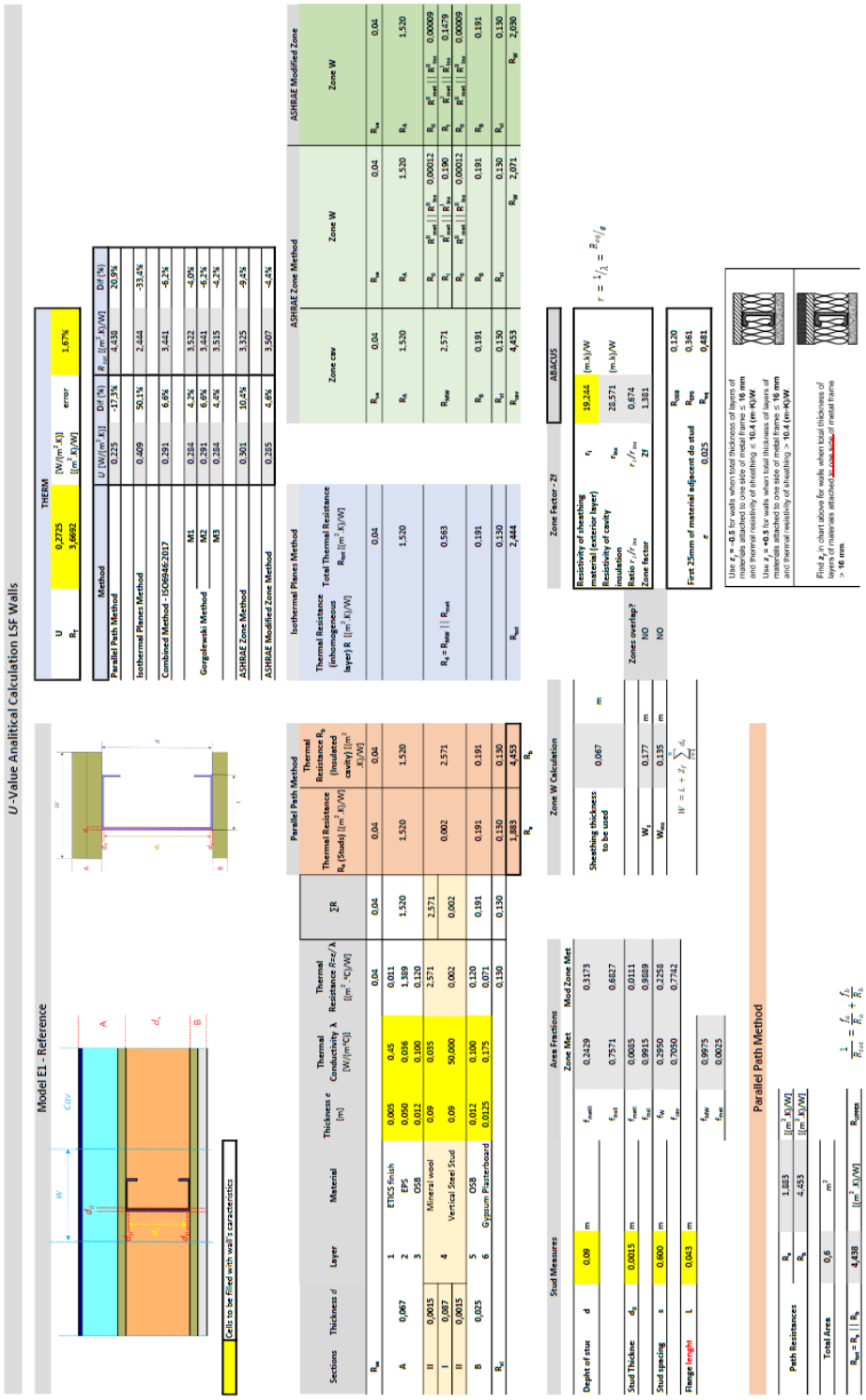

Figure B.1 – Excel spreadsheet used to calculate the *U*-value for wall models.

C ANALYTICAL METHODS AND NUMERICAL SIMULATIONS RESULTS

The Table C.1 summarize the configuration for the parameters that were varied (highlighted on the table) in each model in relation to the reference model, which is the model 9.

Table C.1 – Wall models descriptions, the parameters that were varied and the thermal transmittance for each numerical simulation (THERM).

Parameter	Model	Wall Layers (outer to inner)							ss[1] (mm)	*U*-value [W/(m².K)]
		1	2	3	4		5	6		
Studs	1	EFL[2] (5)	EPS[3] (50)	OSB[4] (12)	MW[5] (90)	C90 **(0.6)**	OSB (12)	GPB[6] (12.5)	600	0.2643
	2	EFL (5)	EPS (50)	OSB (12)	MW (90)	C90 **(1.0)**	OSB (12)	GPB (12.5)	600	0.2691
	3	EFL (5)	EPS (50)	OSB (12)	MW (90)	C90 **(1.2)**	OSB (12)	GPB (12.5)	600	0.2706
	4	EFL (5)	EPS (50)	OSB (12)	MW (90)	C90 **(2.0)**	OSB (12)	GPB (12.5)	600	0.2742
	5	EFL (5)	**EPS(0)**	OSB (12)	MW (90)	C90 **(0.6)**	OSB (12)	GPB (12.5)	600	0.4503
	6	EFL (5)	**EPS(0)**	OSB (12)	MW (90)	C90 **(1.0)**	OSB (12)	GPB (12.5)	600	0.4736
	7	EFL (5)	**EPS(0)**	OSB (12)	MW (90)	C90 **(1.2)**	OSB (12)	GPB (12.5)	600	0.4810
	8	EFL (5)	**EPS(0)**	OSB (12)	MW (90)	C90 **(2.0)**	OSB (12)	GPB (12.5)	600	0.5003
	9*	EFL (5)	EPS (50)	OSB (12)	MW (90)	C90 (1.5)	OSB (12)	GPB (12.5)	600	0.2725
	10	EFL (5)	EPS (50)	OSB (12)	MW (150)	**C150 (1.5)**	OSB (12)	GPB (12.5)	600	0.2236
	11	EFL (5)	EPS (50)	OSB (12)	MW (200)	**C200 (1.5)**	OSB (12)	GPB (12.5)	600	0.1994
	12	EFL (5)	EPS (50)	OSB (12)	MW (170)	**C170 (1.5)**	OSB (12)	GPB (12.5)	600	0.2233
	13	EFL (5)	EPS (50)	OSB (12)	**Air (170)**	**C170 (1.5)**	OSB (12)	GPB (12.5)	600	0.4888
	14	EFL (5)	**EPS(0)**	OSB (12)	MW (170)	**C170 (1.5)**	OSB (12)	GPB (12.5)	600	0.3838
	15	EFL (5)	**EPS (30)**	OSB (12)	**Air (170)**	**C170 (1.5)**	OSB (12)	GPB (12.5)	600	0.6711
	16	EFL (5)	**EPS (20)**	OSB (12)	**Air (170)**	**C170 (1.5)**	OSB (12)	GPB (12.5)	600	0.8247
	17	EFL (5)	**EPS (15)**	OSB (12)	**Air (170)**	**C170 (1.5)**	OSB (12)	GPB (12.5)	600	0.9315
	18	EFL (5)	EPS (50)	OSB (12)	MW (90)	C90 (1.5)	OSB (12)	GPB (12.5)	**300**	0.3199
	19	EFL (5)	EPS (50)	OSB (12)	MW (90)	C90 (1.5)	OSB (12)	GPB (12.5)	**400**	0.2965
	20	EFL (5)	EPS (50)	OSB (12)	MW (90)	C90 (1.5)	OSB (12)	GPB (12.5)	**800**	0.2606
	21	EFL (5)	EPS (50)	OSB (12)	**Air (90)**	C90 (1.5)	OSB (12)	GPB (12.5)	**300**	0.4933
	22	EFL (5)	EPS (50)	OSB (12)	**MW (45)**	C90 (1.5)	OSB (12)	GPB (12.5)	**300**	0.3815
	23	EFL (5)	EPS (50)	OSB (12)	**Air (90)**	C90 (1.5)	OSB (12)	GPB (12.5)	**400**	0.4912
	24	EFL (5)	EPS (50)	OSB (12)	**MW (45)**	C90 (1.5)	OSB (12)	GPB (12.5)	**400**	0.3625
	25	EFL (5)	EPS (50)	OSB (12)	**Air (90)**	C90 (1.5)	OSB (12)	GPB (12.5)	**800**	0.4882
	26	EFL (5)	EPS (50)	OSB (12)	**MW (45)**	C90 (1.5)	OSB (12)	GPB (12.5)	**800**	0.3311
	27	EFL (5)	EPS (50)	OSB (12)	**Air (90)**	C90 **(0.6)**	OSB (12)	GPB (12.5)	600	0.4865
	28	EFL (5)	EPS (50)	OSB (12)	**MW (45)**	C90 **(0.6)**	OSB (12)	GPB (12.5)	600	0.3328
	29	EFL (5)	EPS (50)	OSB (12)	**Air (90)**	C90 **(1.0)**	OSB (12)	GPB (12.5)	600	0.4873

	30	EFL (5)	EPS (50)	OSB (12)	**MW (45)**	C90 **(1.0)**	OSB (12)	GPB (12.5)	600	0.3378
	31	EFL (5)	EPS (50)	OSB (12)	**Air (90)**	C90 **(1.2)**	OSB (12)	GPB (12.5)	600	0.4877
	32	EFL (5)	EPS (50)	OSB (12)	**MW (45)**	C90 **(1.2)**	OSB (12)	GPB (12.5)	600	0.3394
	33	EFL (5)	EPS (50)	OSB (12)	**Air (90)**	C90 **(2.0)**	OSB (12)	GPB (12.5)	600	0.4897
	34	EFL (5)	EPS (50)	OSB (12)	**MW (45)**	C90 **(2.0)**	OSB (12)	GPB (12.5)	600	0.3438
Cavity Insulation	35	EFL (5)	EPS (50)	OSB (12)	**Air (90)**	C90 (1.5)	OSB (12)	GPB (12.5)	600	0.4892
	36	EFL (5)	EPS (50)	OSB (12)	**MW (45)**	C90 (1.5)	OSB (12)	GPB (12.5)	600	0.3419
	37	EFL (5)	EPS (50)	OSB (12)	**Air (150)**	**C150 (1.5)**	OSB (12)	GPB (12.5)	600	0.4888
	38	EFL (5)	EPS (50)	OSB (12)	**MW (75)**	**C150 (1.5)**	OSB (12)	GPB (12.5)	600	0.3048
	39	EFL (5)	EPS (50)	OSB (12)	**Air (200)**	**C200 (1.5)**	OSB (12)	GPB (12.5)	600	0.4884
	40	EFL (5)	EPS (50)	OSB (12)	**MW (100)**	**C200 (1.5)**	OSB (12)	GPB (12.5)	600	0.2845
	41	EFL (5)	EPS (50)	OSB (12)	**MW (85)**	**C170 (1.5)**	OSB (12)	GPB (12.5)	600	0.3049
	42	EFL (5)	EPS (50)	OSB (12)	**AIB[7] (45)**	C90 (1.5)	OSB (12)	GPB (12.5)	600	0.2875
	43	EFL (5)	EPS (50)	OSB (12)	**AIB (90)**	C90 (1.5)	OSB (12)	GPB (12.5)	600	0.2087
	44	EFL (5)	EPS (50)	OSB (12)	**AIB (75)**	**C150 (1.5)**	OSB (12)	GPB (12.5)	600	0.2576
	45	EFL (5)	EPS (50)	OSB (12)	**AIB (150)**	**C150 (1.5)**	OSB (12)	GPB (12.5)	600	0.1709
	46	EFL (5)	EPS (50)	OSB (12)	**AIB (100)**	**C200 (1.5)**	OSB (12)	GPB (12.5)	600	0.2423
	47	EFL (5)	EPS (50)	OSB (12)	**AIB (200)**	**C200 (1.5)**	OSB (12)	GPB (12.5)	600	0.1533
	48	EFL (5)	EPS (50)	OSB (12)	**AIB (85)**	**C170 (1.5)**	OSB (12)	GPB (12.5)	600	0.2641
	49	EFL (5)	EPS (50)	OSB (12)	**AIB (170)**	**C170 (1.5)**	OSB (12)	GPB (12.5)	600	0.1761
Exterior Insulation (ETICS)	50	EFL (5)	**EPS (30)**	OSB (12)	MW (90)	C90 (1.5)	OSB (12)	GPB (12.5)	600	0.3248
	51	EFL (5)	**EPS (80)**	OSB (12)	MW (90)	C90 (1.5)	OSB (12)	GPB (12.5)	600	0.2210
	52	EFL (5)	**EPS(0)**	OSB (12)	MW (90)	C90 (1.5)	OSB (12)	GPB (12.5)	600	0.4910
	53	EFL (5)	**EPS(0)**	OSB (12)	MW (90)	C90 (1.5)	OSB (12)	GPB (12.5)	600	0.4504
	54	EFL (5)	**EPS (20)**	OSB (12)	**Air (90)**	C90 (1.5)	OSB (12)	GPB (12.5)	600	0.8258
	55	EFL (5)	**EPS (10)**	OSB (12)	**MW (45)**	C90 (1.5)	OSB (12)	GPB (12.5)	600	0.5579
	56	EFL (5)	**EPS (15)**	OSB (12)	**Air (90)**	C90 (1.5)	OSB (12)	GPB (12.5)	600	0.9328
	57	EFL (5)	**EPS (5)**	OSB (12)	**MW (45)**	C90 (1.5)	OSB (12)	GPB (12.5)	600	0.6080
	58	EFL (5)	**EPS (25)**	OSB (12)	**MW (45)**	C90 (1.5)	OSB (12)	GPB (12.5)	600	0.4499
	59	EFL (5)	**EPS (30)**	OSB (12)	**Air (90)**	C90 (1.5)	OSB (12)	GPB (12.5)	600	0.6718
	60	EFL (5)	**EPS (80)**	OSB (12)	**Air (90)**	C90 (1.5)	OSB (12)	GPB (12.5)	600	0.3477
	61	EFL (5)	**EPS (25)**	OSB (12)	**Air (90)**	C90 (1.5)	OSB (12)	GPB (12.5)	600	0.7410
	62	EFL (5)	**EPS (30)**	OSB (12)	**MW (45)**	C90 (1.5)	OSB (12)	GPB (12.5)	600	0.4231
	63	EFL (5)	**EPS (80)**	OSB (12)	**MW (45)**	C90 (1.5)	OSB (12)	GPB (12.5)	600	0.2658
	64	EFL (5)	**EPS(0)**	OSB (12)	**MW (45)**	C90 (1.5)	OSB (12)	GPB (12.5)	600	0.6708
	65	EFL (5)	**EPS(0)**	OSB (12)	**AIB (45)**	C90 (1.5)	OSB (12)	GPB (12.5)	600	0.5045
	66	EFL (5)	**ICB[8] (30)**	OSB (12)	MW (90)	C90 (1.5)	OSB (12)	GPB (12.5)	600	0.346
	67	EFL (5)	**ICB (80)**	OSB (12)	MW (90)	C90 (1.5)	OSB (12)	GPB (12.5)	600	0.2463
	68	EFL (5)	**ICB (50)**	OSB (12)	MW (90)	C90 (1.5)	OSB (12)	GPB (12.5)	600	0.2968
Sheathing	69	EFL (5)	EPS (50)	**CWB[9] (12)**	MW (90)	C90 (1.5)	**CWB (12)**	GPB (12.5)	600	0.2934
	70	EFL (5)	EPS (50)	**FCB[10] (12)**	MW (90)	C90 (1.5)	**FCB (12)**	GPB (12.5)	600	0.308
	71	EFL (5)	EPS (50)	**GRC[11] (12)**	MW (90)	C90 (1.5)	**GRC (12)**	GPB (12.5)	600	0.3146

72	EFL (5)	**EPS(0)**	**CWB (12)**	MW (90)	C90 (1.5)	**CWB (12)**	GPB (12.5)	600	0.5794
73	EFL (5)	**EPS(0)**	**FCB (12)**	MW (90)	C90 (1.5)	**FCB (12)**	GPB (12.5)	600	0.6395
74	EFL (5)	**EPS(0)**	**GRC (12)**	MW (90)	C90 (1.5)	**GRC (12)**	GPB (12.5)	600	0.6648
75	EFL (5)	**EPS (20)**	**CWB (12)**	**Air (90)**	C90 (1.5)	**CWB (12)**	GPB (12.5)	600	0.9265
76	EFL (5)	**EPS (20)**	**FCB (12)**	**Air (90)**	C90 (1.5)	**FCB (12)**	GPB (12.5)	600	0.9698
77	EFL (5)	**EPS (20)**	**GRC (12)**	**Air (90)**	C90 (1.5)	**GRC (12)**	GPB (12.5)	600	0.9831
78	EFL (5)	**EPS(0)**	**CWB (12)**	**MW (45)**	C90 (1.5)	**CWB (12)**	GPB (12.5)	600	0.7780
79	EFL (5)	**EPS(0)**	**FCB (12)**	**MW (45)**	C90 (1.5)	**FCB (12)**	GPB (12.5)	600	0.8431
80	EFL (5)	**EPS(0)**	**GRC (12)**	**MW (45)**	C90 (1.5)	**GRC (12)**	GPB (12.5)	600	0.8691

***** Reference Wall; [1]SS – Stud Spacing; [2]EFL – ETICS Finish Layer; [3]EPS - Expanded Polystyrene; [4]OSB - Oriented Strand Board; [5]MW - Mineral Wool; [6]GPB - Gypsum Plaster Board; [7]AIB – Aerogel Insulation Blanket; [8]ICB – Insulation Cork Board; [9]CWB - Cement Wood Board; [10]FCB - Fiber Cement Board; [11]GRB - Glass-fiber Reinforced Board.

The U-value results for all analytical methods for each of the 80 models are represented in Table C.2, as well as, the reference U-value from the numerical simulation from THERM.

Table C.2 - U- values from analytical methods and the numerical simulation.

Model	**U-value [W/(m^2.K)]**						
	ISO 6946	**Gorgolewsky**			**ASHRAE Zone Method**	**Modified Zone Method**	**Numerical THERM**
		Met. 1	**Met. 2**	**Met. 3**			
1	0.271	0.257	0.271	0.258	0.286	0.275	0.264
2	0.282	0.272	0.282	0.272	0.295	0.281	0.269
3	0.286	0.277	0.286	0.278	0.298	0.283	0.271
4	0.296	0.292	0.296	0.293	0.304	0.287	0.274
5	0.435	0.433	0.500	0.434	0.484	0.457	0.450
6	0.466	0.495	0.559	0.496	0.514	0.478	0.474
7	0.477	0.521	0.581	0.523	0.524	0.484	0.481
8	0.506	0.601	0.641	0.604	0.546	0.497	0.500
9*	0.291	0.284	0.291	0.284	0.301	0.285	0.273
10	0.223	0.229	0.223	0.234	0.248	0.245	0.224
11	0.187	0.199	0.187	0.207	0.220	---	0.199
12	0.207	0.216	0.207	0.235	0.246	0.243	0.223
13	0.488	0.488	0.488	0.488	0.489	0.490	0.489
14	0.295	0.358	0.377	0.413	0.416	0.399	0.384
15	0.669	0.669	0.669	0.669	0.672	0.673	0.671
16	0.821	0.821	0.821	0.821	0.825	0.827	0.825
17	0.927	0.927	0.927	0.927	0.932	0.934	0.932
18	0.302	0.303	0.324	0.351	0.377	0.346	0.320
19	0.298	0.295	0.318	0.316	0.339	0.315	0.297
20	0.285	0.275	0.285	0.269	0.282	0.270	0.261

21	0.492	0.492	0.492	0.492	0.497	0.499	0.493
22	0.366	0.349	0.383	0.382	0.412	0.389	0.382
23	0.491	0.491	0.491	0.491	0.494	0.496	0.491
24	0.362	0.344	0.378	0.359	0.383	0.366	0.363
25	0.488	0.488	0.488	0.488	0.490	0.490	0.488
26	0.351	0.332	0.351	0.327	0.341	0.332	0.331
27	0.487	0.487	0.487	0.487	0.488	0.489	0.487
28	0.339	0.321	0.339	0.321	0.344	0.336	0.333
29	0.488	0.488	0.488	0.488	0.490	0.490	0.487
30	0.348	0.330	0.348	0.330	0.351	0.341	0.338
31	0.489	0.489	0.489	0.489	0.491	0.491	0.488
32	0.352	0.333	0.352	0.333	0.353	0.342	0.339
33	0.490	0.490	0.490	0.490	0.492	0.494	0.490
34	0.360	0.342	0.360	0.343	0.358	0.345	0.344
35	0.489	0.489	0.489	0.489	0.491	0.492	0.489
36	0.356	0.337	0.356	0.337	0.355	0.344	0.342
37	0.488	0.488	0.488	0.488	0.490	0.491	0.489
38	0.299	0.288	0.299	0.292	0.306	0.311	0.305
39	0.487	0.487	0.487	0.487	0.489	---	0.488
40	0.265	0.260	0.265	0.267	0.278	---	0.285
41	0.284	0.276	0.284	0.292	0.302	0.307	0.305
42	0.291	0.290	0.291	0.291	0.299	0.275	0.288
43	0.214	0.237	0.214	0.238	0.244	0.215	0.209
44	0.229	0.243	0.229	0.249	0.306	0.247	0.258
45	0.153	0.188	0.153	0.195	0.202	0.187	0.171
46	0.194	0.217	0.194	0.228	0.226	---	0.242
47	0.124	0.162	0.124	0.174	0.181	---	0.153
48	0.214	0.232	0.214	0.257	0.252	0.248	0.264
49	0.140	0.177	0.140	0.207	0.205	0.191	0.176
50	0.347	0.349	0.347	0.350	0.353	0.335	0.325
51	0.234	0.224	0.234	0.224	0.248	0.235	0.221
52	0.490	0.555	0.607	0.557	0.534	0.490	0.491
53	0.462	0.510	0.566	0.511	0.494	0.455	0.450
54	0.826	0.826	0.826	0.826	0.829	0.831	0.826
55	0.589	0.581	0.589	0.582	0.561	0.549	0.558
56	0.934	0.934	0.934	0.934	0.936	0.939	0.933
57	0.641	0.643	0.641	0.645	0.616	0.604	0.608
58	0.472	0.454	0.472	0.455	0.459	0.450	0.450
59	0.368	0.376	0.368	0.377	0.381	0.358	0.346
60	0.261	0.252	0.261	0.252	0.282	0.264	0.246
61	0.316	0.313	0.316	0.314	0.333	0.312	0.297
62	0.672	0.672	0.672	0.672	0.674	0.676	0.672
63	0.348	0.348	0.348	0.348	0.349	0.349	0.348
64	0.741	0.741	0.741	0.741	0.744	0.746	0.741

65	0.443	0.424	0.443	0.425	0.433	0.425	0.423
66	0.274	0.259	0.274	0.260	0.280	0.275	0.266
67	0.705	0.722	0.827	0.724	0.695	0.664	0.671
68	0.493	0.599	0.630	0.602	0.529	0.482	0.505
69	0.302	0.297	0.302	0.297	0.315	0.296	0.293
70	0.307	0.302	0.307	0.302	0.321	0.301	0.308
71	0.308	0.303	0.308	0.304	0.322	0.302	0.315
72	0.525	0.616	0.661	0.619	0.619	0.551	0.579
73	0.540	0.643	0.684	0.646	0.661	0.578	0.640
74	0.544	0.651	0.691	0.654	0.675	0.587	0.665
75	0.927	0.927	0.927	0.927	0.930	0.929	0.927
76	0.969	0.969	0.969	0.969	0.973	0.972	0.970
77	0.982	0.982	0.982	0.982	0.986	0.989	0.983
78	0.777	0.819	0.929	0.822	0.801	0.747	0.778
79	0.808	0.862	0.972	0.865	0.853	0.784	0.843
80	0.817	0.876	0.985	0.878	0.870	0.795	0.869